RESEARCH ARTICLE

C. Lacasse · H. Sigurdsson · S. N. Carey ·
H. Jóhannesson · L. E. Thomas · N. W. Rogers

Bimodal volcanism at the Katla subglacial caldera, Iceland: insight into the geochemistry and petrogenesis of rhyolitic magmas

Abstract The Katla subglacial caldera is one of the most active and hazardous volcanic centres in Iceland as revealed by its historical volcanic activity and recent seismic unrest and magma accumulation. A petrologic and geochemical study was carried out on a suite of mid-Pleistocene to Recent lavas and pyroclastic rocks originated from the caldera. The whole series is characterised by a bimodal composition, including Fe-Ti transitional alkali basalts and mildly alkalic rhyolites. Variations in trace-element composition amongst the basalts and rhyolites show that their chemical differentiation was mainly controlled by fractional crystallisation and possible assimilation. The petrology and chemistry of the few intermediate extrusive rocks show that they were derived from magma mingling or hybridisation. The absence of extrusive rocks of true intermediate magmatic composition and the occurrence of amphibole-bearing felsic xenoliths support the hypothesis of partial melting of the hydrated basalt crust as the main process leading to the generation of rhyolites. The $^{143}Nd/^{144}Nd$ and $^{87}Sr/^{86}Sr$ values of Katla volcanic rocks fit the general isotopic array defined by late Quaternary to Recent lavas from Iceland. A few rock specimens are distinguished by low $^{143}Nd/^{144}Nd$ values suggesting assimilation and mixing of much older crustal material. Despite their similar whole-rock chemical compositions, the postglacial rhyolitic extrusives differ from the felsic xenoliths by their glass composition and the absence of amphibole. This, together with the general chemical trend of volcanic glasses, indicates that the postglacial rhyolitic extrusives were probably derived by a process involving late reheating and partial melting of crustal material by intrusion of basaltic magmas.

Keywords Katla · Iceland · Subglacial caldera ·
Bimodal volcanism · Rhyolite · Basalt · Magma mixing

C. Lacasse (✉)
5, allée des Flandres,
F-54390 Frouard, France
e-mail: christian.lacasse@wanadoo.fr
Tel.: +33-676194505

H. Sigurdsson · S. N. Carey
Graduate School of Oceanography, University of Rhode Island,
Narragansett Bay Campus,
Narragansett, RI 02882-1197, USA

H. Jóhannesson
ISOR, Iceland GeoSurvey,
Grensásvegur 9,
IS-108 Reykjavík, Iceland

L. E. Thomas · N. W. Rogers
Department of Earth Sciences, The Open University,
Walton Hall,
Milton Keynes, MK7 6AA, UK

Introduction

Iceland is identified as the main source of major rhyolitic explosive eruptions from the 0–6 Ma deep-sea sediment record of tephra fall layers in the North Atlantic and Arctic Oceans (Lacasse and Garbe-Schönberg 2001). The volume of erupted magma for each eruption probably exceeded several km^3, based on estimates from the few constrained events. This observation suggests that the volume of exposed silicic rocks in Iceland, reported about 10–12% of the total volume (e.g. Sæmundsson 1979), underestimates the full contribution of rhyolitic melts in the crustal evolution and eruptive history of Iceland.

Two main hypotheses have been suggested for the petrogenesis of Icelandic rhyolites. The first petrogenetic model to be proposed was based on one-stage fractional crystallisation of a basaltic magma, by extraction of an assemblage of mineral phases (e.g. plagioclase, K-feldspar, clinopyroxene, titanomagnetite, ilmenite, apatite) that remain present in the derived silicic rocks (Carmichael 1964; Wood 1978; MacDonald et al. 1990; Furman et al. 1992). Multiple-stage processes involving fractional crystallisation, magma mixing and hybridisation were also

suggested (Sigurdsson and Sparks 1981; Blake 1984; McGarvie 1984; McGarvie et al. 1990).

The second main petrogenetic model implies partial melting of some parts of the Icelandic crust, i.e. plagiogranite or hydrothermally altered basalt (amphibolite), along the Eastern Rift Zone (ERZ) (Sigurdsson 1977; Oskarsson et al. 1982, 1985; Sigmarsson et al. 1991). The main support for this model lies in the occurrence of quenched xenoliths in various stages of remelting. The xenoliths, mainly leucocratic in composition (trondhjemite, granodiorite), represent fragments of country rock which have been incorporated during uprise or eruption. This second petrogenetic model for Icelandic rhyolites was implemented by Gunnarsson et al. (1998) following a study of the Torfajökull central volcano located at the southern tip of the Veidivötn fissure swarm. The volcano erupted a total volume of ~225 km³ of silicic extrusives covering an area of ~450 km² that is mainly ice-free at present. The distinct chemical composition of the postglacial rhyolitic units (domes) was interpreted to be the result of heterogeneous crustal melting and wall rock collapse, leading to the segregation of silicic pods and lenses in the upper part of gabbroic intrusives (Gunnarsson et al. 1998).

The most recent of these major rhyolitic eruptions in Iceland occurred about 11,980 years BP from the Katla subglacial caldera under the Mýrdalsjökull ice cap in southern Iceland (Figs. 1 and 2), and generated at least 6–7 km³ of pyroclastic material (Lacasse et al. 1995). The eruption produced massive pyroclastic falls and flows on land (i.e. Sólheimar ignimbrite), glacier meltwater floods (jökulhlaups), and widespread airborne fallout of fine ash that is known to be recorded in the marine and terrestrial records as Ash Zone 1 and the Vedde Ash, respectively. Fieldwork conducted on ice-free rock exposures (nunataks) of the Mýrdalsjökull ice cap in summer 2002 brought new evidence that this prehistoric eruption formed more extensive and thicker proximal pyroclastic deposits of rhyolitic pumice and obsidian than previously thought.

In spite of recent seismic unrest and inflation recorded at the caldera since 1999 (Einarsson and Brandsdóttir 2000; Sturkell et al. 2003a,b), no geochemical study of its rock series has been carried out to date, with the exception of unpublished work by Hildebrand et al. (1998). As a future major explosive silicic eruption is likely to be of significant environmental impact (Lacasse et al. 2002), a geochemical investigation of exposed lavas and pyroclastic rocks erupted from the Katla subglacial caldera is presented. We emphasise the important silicic end-member in this study and discuss its petrogenesis in the context of the current debate on the generation of rhyolites in Iceland. The results of our geochemical and petrographic studies clearly support the evidence of bimodal volcanism and magma mixing at the Katla caldera, and bring an insight into the petrogenetic link between crustal felsic xenoliths and rhyolitic extrusives.

Geological background

Tectonics and geology of the Katla volcanic system

The Katla subglacial caldera is part of the Katla volcanic system, a component of the Southern Transgressive Zone (STZ) in Iceland. The caldera is fed by a fissure swarm that includes the 1,100-year-old Eldgjá fissure (Jakobsson 1979; Fig. 1). The Katla caldera is almost entirely covered by an ice cap, restricting its geological investigation to nunataks and preserved pyroclastic deposits (Fig. 2). Previous petrological and geochemical studies have been mainly restricted to postglacial basaltic lavas and basaltic to rhyolitic tephras erupted from the Katla caldera and along the associated Eldgjá eruptive fissure (e.g. Jakobsson 1979; Meyer et al. 1985; Lacasse et al. 1995; Larsen 2000; Larsen et al. 2001; Thordarson et al. 2001; Oladóttir et al. 2005; Sigmarsson et al. 2005). Basalt volcanism is reported to have occurred from the caldera since the middle or late Pleistocene, forming mainly hyaloclastites, subaerial lava flows and tuffs (Jakobsson 1979; Hildebrand et al. 1998). As a result of the southward propagation of the STZ into 2–3-My-old lithosphere (Meyer et al. 1985), Katla volcanic rocks consist of transitional-alkali Fe-Ti basalts, intermediate and silicic products. The transitional-alkali basalts are characterised by a narrow compositional range throughout both the Pleistocene and Holocene, and are invariably very
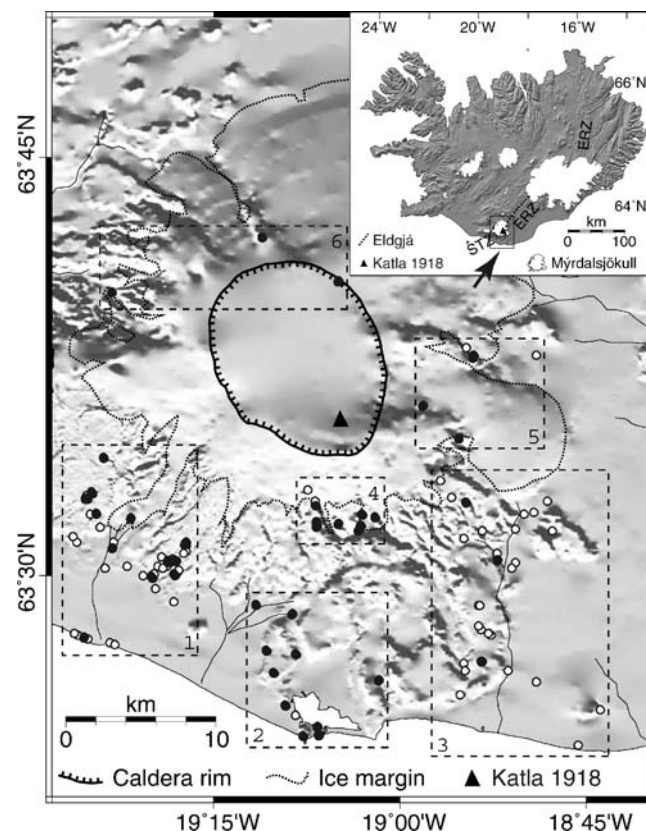

Fig. 1 Location map of sampling areas (1–6) and localities in the Mýrdalsjökull area. Filled and open symbols, rock samples with and without XRF whole-rock analysis, respectively

Fig. 2 Sub-ice topography of the Katla caldera under the Mýrdalsjökull ice cap revealed by radio echo sounding (Björnsson et al. 2000), with localities (*1A–6C*) of exposed rhyolitic rocks and pyroclastic deposits
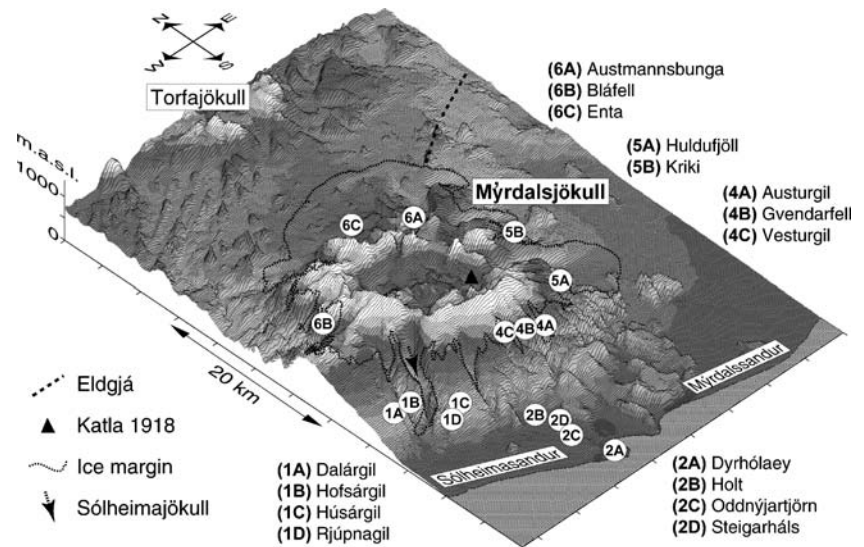
high in TiO_2 (4–5 wt%). Late Quaternary felsic extrusives were first described by Robson (1957) and Sigurdsson (1970) as forming a circle of rhyolitic ice-free exposures around the Katla caldera. Although the rhyolites are suggested to result from magmatic differentiation of Fe-Ti basalt magmas at crustal levels (Hildebrand et al. 1998), no detailed petrogenetic model has been proposed for their origin.

Topography and past eruptions of the Katla caldera

The topography of the subglacial caldera underlying the Mýrdalsjökull ice cap was mapped in detail by Björnsson et al. (2000) by radio echo soundings. The three-dimensional map reveals a 14-km diameter caldera, encircling an area of 100 km^2 and 600–750 m deep (Fig. 2). The rim of the caldera reaches about 1,380 m a.s.l. (above sea level) and is carved by three major glaciers, e.g. the Sólheimajökull glacier in the south. In addition to individual peaks, 750 to ~1,100 m high, several major subglacial ridges are shown radiating out from the caldera rim, one to the west towards Eyjafjallajökull volcano and a second one to the east. The topographic map also reveals a linear depression, 1.5 km wide and 200–250 m deep, striking northeast towards the volcanic fissure Eldgjá. Most of the topographic highs are thought to have formed in subglacial eruptions, either on the caldera floor or along the rim of the caldera.

The most recent event may have been a small subglacial eruption in the summer of 1999 when depressions (cauldrons) were formed on the surface of the Mýrdalsjökull ice cap as a result of induced geothermal melting at its base (Science Institute website: http://www.raunvis.hi.is/%7Emtg/emyrdj.htm, accessed 01.12.03). The Katla eruption in October 1918 was the latest that was visually observed melting through the Mýrdalsjökull ice cap, lasting 24 days and generating large meltwater floods (jökulhlaups) and an eruption column ~14 km high (Larsen 2000). Past volcanism at the caldera has been mainly reconstructed from the recovery and study of tephra fall layers in soil, marine sediments, and ice cores (Grönvold et al. 1995; Lacasse et al. 1995, 1998; Larsen 2000; Larsen et al. 2001; Oladóttir et al. 2005). This tephrochronological framework was complemented by studies of extended and thick volcaniclastic deposits resulting from subglacial eruptions and associated jökulhlaups (Jónsson 1982; Maizels 1991; Larsen 2000). However, results from these studies only illustrate part of the volcanic activity at the caldera and only a fraction of the volume of erupted magma. Age and volume estimates of basaltic lava flows and rhyolitic domes erupted subglacially or subaerially, for example, are poorly constrained. Only two major postglacial basaltic lava flows are known to have been erupted from the associated >75-km-long eruptive fissure Eldgjá and adjacent vents, i.e. the ~6,800 ^{14}C years BP Hólmsá lavas and the AD 934–940 years Eldgjá lavas (~19 km^3; Larsen 2000; Thordarson et al. 2001). Holocene volcanism from the caldera itself is mainly recorded by the deposition of tephra falls and volcanogenic jökulhlaups (Larsen 2000; Oladóttir et al. 2005). For the last 8,400 years, eruption frequency varied between 10 and 16 eruptions per 1,000 years. At least 20 eruptions were documented for the last 11 centuries, all of basaltic composition and giving rise to less than 1.5 km^3 of tephra, with an average repose period of ~50 years (since AD 1,500) and duration between 2 weeks and 4 months. At least twelve silicic eruptions, each producing less than 0.5 km^3 of tephra of trachydacitic to dacitic glass composition (Na_2O+K_2O=7.6–8.0 wt% for SiO_2=66.4–66.8 wt%), occurred in the period between ~1,700 ^{14}C years BP and ~6,600 ^{14}C years BP (Larsen et al. 2001). The largest explosive eruption known in the Katla caldera formed the rhyolitic Sólheimar ignimbrite on its southern slope, and the widespread Vedde Ash and Ash Zone 1 in the North Atlantic region (e.g. Lacasse et al. 1995). The recovery of a correlative distal ash fall layer in a Greenland ice core dates this event at ~11,980 cal years BP (Grönvold et al. 1995). The distal tephra fallout covered an area encompassing Iceland, SE Greenland, the Greenland-

Table 1 Selected whole-rock analyses of volcanic rocks from the Katla subglacial caldera

Sampling area	1	1	1	1	1	1	1	1
Locality	E. Rjúpnagil	W. Hofsárgil	Sólheimajökull	Skógasandur	W. Hofsárgil	W. Hofsárgil	E. Rjúpnagil	Sjónarholl
Locality No.	5 (OU-02)	11 (OU-02)	33 (OU-02)	32 (OU-02)	11 (OU-02)	11 (OU-02)	23 (OU-02)	2 (URI-95)
Sample No.	KAT02-7	KAT02-12a	KAT02-43	KAT02-40	KAT02-12b	KAT02-12c	KAT02-27b	IC95-06
Exposure	Columnar lava	PFD	Glacier surf.	Flood deposit	PFD	PFD	PFD	Scree
Rock	Basalt	Basalt clast	Lapilli	Lapilli	Pumice	Bulk matrix	Pumice	Xenolith
Major elements (XRF, wt%)								
SiO_2	46.38	47.35	47.80	48.07	67.76	68.19	68.72	69.10
TiO_2	4.28	4.33	4.36	4.52	0.34	0.39	0.33	0.45
Al_2O_3	13.48	13.41	13.08	13.22	13.76	13.60	13.50	13.35
Fe_2O_3	17.15	16.33	16.59	16.87	4.57	4.74	4.45	5.19
MnO	0.22	0.23	0.24	0.23	0.15	0.15	0.14	0.17
MgO	5.53	4.56	4.89	5.01	0.23	0.29	0.21	0.41
CaO	10.46	9.14	9.51	9.69	1.43	1.61	1.43	1.58
Na_2O	2.73	3.18	2.99	2.94	5.23	5.41	5.34	5.40
K_2O	0.55	0.77	0.81	0.83	3.31	3.27	3.39	3.40
P_2O_5	0.50	0.63	0.69	0.58	0.05	0.06	0.05	0.07
LOI	−0.50	−0.24	−0.69	−0.64	3.19	2.25	2.30	0.59
Total	100.78	99.70	100.26	101.32	100.01	99.96	99.87	99.73
Trace elements (XRF, ppm)								
Rb	10	12	17	16	76	75	78	80
Sr	447	513	451	431	131	151	132	173
Y	39	47	45	44	102	94	96	86
Zr	224	275	266	267	955	910	935	868
Nb	30	39	38	38	121	115	119	115
Ba	196	294	226	216	673	657	658	665
Trace elements (ICPMS, ppm)								
Li	6	10	7	6	23	19	22	16
B	3	4	2	10	6	12	12	
Sc	33	25	33	17	7	5	5	5
Ti	26,602	25,711	26,843	26,365	2,031	2,129	1,908	2,687
V	461	321	370	402	1	5	1	1
Cr	29	1	7	2	2	1	2	1
Co	52	40	47	46	1	1	1	1
Ni	45	6	19	19	0	1	0	0
Cu	112	14	61	58	7	5	5	4
Zn	151	204	150	150	170	164	171	158
Rb	10	11	16	12	79	65	76	76
Sr	441	474	458	393	138	137	132	173
Y	38	44	46	36	105	78	94	75

Table 1 (continued)

	1	1	1	1	1	1	1	1
Sampling area	E. Rjúpnagil	W. Hofsárgil	Sólheimajökull	Skógasandur	W. Hofsárgil	W. Hofsárgil	E. Rjúpnagil	Sjónarholl
Locality	5 (OU-02)	11 (OU-02)	33 (OU-02)	32 (OU-02)	11 (OU-02)	11 (OU-02)	23 (OU-02)	2 (URI-95)
Locality No.	KAT02-7	KAT02-12a	KAT02-43	KAT02-40	KAT02-12b	KAT02-12c	KAT02-27b	IC95-06
Sample No.	Columnar lava	PFD	Glacier surf.	Flood deposit	PFD	PFD	PFD	Scree
Exposure	Basalt	Basalt clast	Lapilli	Lapilli	Pumice	Bulk matrix	Pumice	Xenolith
Rock								
Zr	224	263	261	248	973	818	921	249
Nb	31	40	38	36	130	110	122	121
Mo	1	1	2	2	6	5	6	6
Sn	2	2	2	2	8	7	7	7
Sb	0	0	0	0	0	0	0	0
Cs	0	0	0	0	1	1	1	1
Ba	161	237	198	181	666	594	644	643
La	23	31	29	25	89	66	83	79
Ce	55	71	70	62	194	149	184	170
Pr	8	10	10	8	26	19	24	21
Nd	32	40	40	34	90	69	83	80
Sm	8	10	10	9	20	16	19	17
Eu	3	3	3	3	4	3	4	4
Gd	9	11	11	9	19	15	18	16
Tb	1	1	2	1	3	2	3	3
Dy	7	8	8	7	17	14	16	14
Ho	1	2	2	1	4	3	3	3
Er	3	4	4	4	10	8	9	7
Yb	3	3	3	3	9	7	8	6
Lu	0	0	0	0	1	1	1	1
Hf	5	6	6	6	23	20	22	6
Ta	2	3	2	2	8	6	7	7
Pb	2	2	2	2	8	6	7	5
Th	2	3	3	2	13	9	12	9
U	1	1	1	1	4	3	4	2
Isotopic ratios (TIMS)								
$^{87}Sr/^{86}Sr$	0.703390 (±3)		0.703353 (±4)		0.703446 (±6)			
$^{143}Nd/^{144}Nd$	0.512959 (±7)		0.512883 (±10)		0.512813 (±5)			

Table 1 (continued)

Sampling area	1	1	1	1	2	2	2	3
Locality	W. Húsargil	E. Rjúpnagil	E. Húsargil	W. Húsargil	Holt	Holt	Oddnýjartjörn	Kerlingardalur
Locality No.	30 (OU-02)	23 (OU-02)	35 (OU-02)	29 (OU-02)	59 (URI-95)	59 (URI-95)	107 (URI-95)	65 (URI-95)
Sample No.	KAT02-39	KAT02-27a	KAT02-45	KAT02-37b	IC95-85	IC95-83	IC95-155	IC95-97
Exposure	Scree	PFD	Scree	Scree	Flood deposit	Flood deposit	Interbed layer	Spatter deposit
Rock	Pumice	Obsidian	Pumice	Xenolith	Scoria	Volcanic bomb	Tephra	Scoria
Major elements (XRF, wt%)								
SiO_2	69.59	69.94	70.36	70.77	55.90	59.85	66.88	47.55
TiO_2	0.34	0.33	0.34	0.29	2.87	2.04	0.64	4.21
Al_2O_3	13.46	13.46	13.59	13.47	13.34	13.49	14.03	13.53
Fe_2O_3	4.54	4.50	4.56	4.38	12.16	9.95	5.34	16.31
MnO	0.14	0.15	0.15	0.14	0.20	0.20	0.14	0.24
MgO	0.25	0.23	0.26	0.14	3.15	2.19	0.33	4.55
CaO	1.46	1.43	1.50	1.30	6.50	4.97	1.32	9.13
Na_2O	5.52	5.45	5.51	5.70	3.85	4.47	5.11	3.19
K_2O	3.37	3.43	3.42	3.04	1.79	2.22	3.24	0.79
P_2O_5	0.06	0.05	0.06	0.04	0.35	0.37	0.19	0.68
LOI	1.14	0.29	0.21	0.58	-0.13	-0.16	3.06	0.14
Total	99.87	99.25	99.95	99.87	99.98	99.60	100.28	100.30
Trace elements (XRF, ppm)								
Rb	80	81	79	73	38	50		17
Sr	136	136	140	123	335	311		521
Y	97	98	97	96	63	74		48
Zr	930	945	929	878	516	626		288
Nb	119	120	119	117	68	80		42
Ba	681	666	675	702	401	478		258
Trace elements (ICPMS, ppm)								
Li	22	23	23	9	13	16	21	7
B	10	9	9				4	
Sc	6	6	7	4			7	
Ti	2,048	1,965	2,042	1,688	17,441	12,282	3,729	25,319
V	3	1	2	1	250	143	28	306
Cr	1	1	5	2	2	2	3	1
Co	1	1	1	1	31	18	4	38
Ni	0	0	1	0	15	8	2	4
Cu	5	6	6	4	39	22	11	18
Zn	182	184	184	163	162	178	180	159
Rb	79	81	80	71	38	47	72	17
Sr	136	138	142	125	346	326	117	514
Y	96	98	97	82	63	75	87	47

Table 1 (continued)

Sampling area	1	1	1	1	2	2	2	3
Locality	W. Húsargil	E. Rjúpnagil	E. Húsargil	W. Húsargil	Holt	Holt	Oddnýjartjörm	Kerlingardalur
Locality No.	30 (OU-02)	23 (OU-02)	35 (OU-02)	29 (OU-02)	59 (URI-95)	59 (URI-95)	107 (URI-95)	65 (URI-95)
Sample No.	KAT02-39	KAT02-27a	KAT02-45	KAT02-37b	IC95-85	IC95-83	IC95-155	IC95-97
Exposure	Scree	PFD	Scree	Scree	Flood deposit	Flood deposit	Interbed layer	Spatter deposit
Rock	Pumice	Obsidian	Pumice	Xenolith	Scoria	Volcanic bomb	Tephra	Scoria
Zr	932	949	936	397	518	621	839	282
Nb	124	126	124	124	77	92	133	46
Mo	6	6	6	4			5	
Sn	7	8	7	9			8	
Sb	0	0	0	0	0	0	0	0
Cs	1	1	1	1	1	1	1	0
Ba	661	678	667	657	355	436	595	206
La	85	87	85	86	51	62	78	33
Ce	187	190	187	187	109	131	181	73
Pr	24	24	24	23	14	17	23	10
Nd	84	86	84	89	58	69	80	45
Sm	19	19	19	19	13	16	18	11
Eu	4	4	4	4	4	4	3	4
Gd	18	19	18	17	13	15	17	11
Tb	3	3	3	3	2	2	3	2
Dy	16	16	16	15	11	13	15	9
Ho	3	3	3	3	2	3	3	2
Er	9	9	9	8	6	7	9	4
Yb	8	8	8	6	5	6	8	3
Lu	1	1	1	1	1	1	1	0
Hf	22	23	22	10	12	14	21	7
Ta	7	7	7	7	4	5	9	3
Pb	7	7	7	6	4	5	8	3
Th	12	12	12	10	6	8	12	3
U	4	4	4	2	2	2	4	1
Isotopic ratios (TIMS)								
$^{87}Sr/^{86}Sr$			0.703441 (±30)	0.703398 (±3)				
$^{143}Nd/^{144}Nd$			0.512886 (±6)	0.512923 (±6)				

Table 1 (continued)

	3	4	4	4	4	4	4	4
Sampling area								
Locality	Thakgil	Austurgil	Austurgil	Austurgil	Stórihryggur	Austurgil	Vesturgil	Vesturgil
Locality No.	22 (URI-95)	37 (URI-95)	37 (URI-95)	38 (URI-95)	94 (URI-95)	37 (URI-95)	91 (URI-95)	91 (URI-95)
Sample No.	IC95-37	IC95-67	IC95-66	IC95-74	IC95-139	IC95-68	IC95-136A	IC95-136B
Exposure	PFD	Interbed layer	Interbed layer	Hayloclastite	Hyaloclastite	Interbed layer	PFD	PFD
Rock	Granophyre	Lapilli	Tuff	Basalt	Basalt	Bulk matrix	Obsidian	Pumice
Major elements (XRF, wt%)								
SiO_2	69.75	47.76	47.86	48.51	50.88	51.34	65.32	65.49
TiO_2	0.36	4.44	4.36	3.89	2.92	3.46	0.81	0.79
Al_2O_3	13.42	13.25	13.27	13.70	13.23	13.37	13.78	13.75
Fe_2O_3	4.75	17.10	16.34	15.59	15.93	14.10	7.70	7.49
MnO	0.14	0.22	0.23	0.22	0.32	0.21	0.21	0.20
MgO	0.25	5.21	4.64	4.42	3.27	4.03	0.80	0.77
CaO	1.42	9.97	9.18	9.21	7.64	8.03	2.96	2.82
Na_2O	5.68	2.85	3.01	3.19	3.83	3.24	5.22	5.19
K_2O	3.31	0.75	0.82	0.86	1.11	1.24	2.74	2.78
P_2O_5	0.05	0.48	0.55	0.59	1.25	0.49	0.26	0.25
LOI	0.37	−0.55	−0.70	−0.20	−0.69	0.32	0.08	0.32
Total	99.49	101.49	99.56	99.99	99.69	99.83	99.87	99.85
Trace elements (XRF, ppm)								
Rb	76	15	15	17	22	27	64	65
Sr	149	431	469	477	544	405	283	272
Y	97	39	43	45	67	52	88	89
Zr	837	251	280	273	468	376	798	805
Nb	122	34	39	39	49	50	102	103
Ba	637	187	225	225	305	286	569	588
Trace elements (ICPMS, ppm)								
Li	9	6	7	7	9	9	17	18
B	1	1	1	1		1	4	4
Sc	4	24	23	23		22	5	6
Ti	2,133	26,475	26,702	23,413	17,885	20,797	4,709	4,565
V	1	441	352	307	99	280	11	11
Cr	1	9	1	21	9	14	1	0
Co	1	50	44	40	21	37	4	4
Ni	0	35	9	16	5	16	0	0
Cu	6	101	26	38	48	42	5	5
Zn	144	152	156	164	196	166	190	199
Rb	76	9	16	16	21	25	38	62
Sr	155	407	476	488	549	408	239	260
Y	86	30	44	43	67	51	57	85

Table 1 (continued)

	Thakgil	Austurgil	Austurgil	Austurgil	Stórihryggur	Austurgil	Vesturgil	Vesturgil
Sampling area	3	4	4	4	4	4	4	4
Locality No.	22 (URI-95)	37 (URI-95)	37 (URI-95)	38 (URI-95)	94 (URI-95)	37 (URI-95)	91 (URI-95)	91 (URI-95)
Sample No.	IC95-37	IC95-67	IC95-66	IC95-74	IC95-139	IC95-68	IC95-136A	IC95-136B
Exposure	PFD	Interbed layer	Interbed layer	Hayloclastite	Hyaloclastite	Interbed layer	PFD	PFD
Rock	Granophyre	Lapilli	Tuff	Basalt	Basalt	Bulk matrix	Obsidian	Pumice
Zr	408	247	277	270	460	366	698	708
Nb	132	36	43	40	55	53	103	104
Mo	10	2		2		2	5	5
Sn	9	2		2		3	6	6
Sb	0	0	0	0	0	0	0	0
Cs	1	0	0	0	0	0	1	1
Ba	664	176	194	209	282	273	532	561
La	93	24	29	31	47	38	51	72
Ce	197	59	66	73	108	88	124	162
Pr	25	8	9	10	16	12	16	21
Nd	94	33	40	41	70	46	61	76
Sm	19	8	10	10	17	11	14	18
Eu	4	3	3	3	6	3	4	4
Gd	18	9	10	11	17	11	14	17
Tb	3	1	1	2	2	2	2	3
Dy	15	7	8	8	13	9	12	15
Ho	3	1	2	2	2	2	2	3
Er	8	3	4	4	6	5	7	8
Yb	6	2	3	3	5	4	6	7
Lu	1	0	0	0	1	1	1	1
Hf	10	6	6	6	10	9	17	17
Ta	8	3	3	2	3	3	6	6
Pb	6	2	2	2	2	3	5	6
Th	11	2	3	3	4	4	6	9
U	3	1	1	1	1	1	2	3
Isotopic ratios (TIMS)								
$^{87}Sr/^{86}Sr$	0.703369 (±3)							
$^{143}Nd/^{144}Nd$	0.512935 (±1)							

Table 1 (continued)

Sampling area	4	4	4	4	5	5	5	5
Locality	Austurgil	Austurgil	Gvendarfell	Austurgil	Near Huldufjöll	Kriki	Near Huldufjöll	Huldufjöll
Locality No.	38 (URI-95)	37 (URI-95)	97 (URI-95)	36 (URI-95)	1 (IMNH)	87 (URI-95)	2 (IMNH)	3 (IMNH)
Sample No.	IC95-75	IC95-65	IC95-142	IC95-60	KAT01-A	IC95-132	KAT01-B	KAT04
Exposure	Interbed layer	Interbed layer	Columnar lava	Interbed breccia	Nunatak	Scree	Nunatak	Nunatak
Rock	Tephra	Tephra	Obsidian	Obsidian	Pumice	Obsidian	Obsidian	Obsidian
Major elements (XRF, wt%)								
SiO_2	68.00	68.21	69.59	70.11	68.56	70.13	70.40	70.93
TiO_2	0.35	0.34	0.36	0.37	0.35	0.29	0.32	0.29
Al_2O_3	13.23	12.99	13.57	13.51	13.00	13.36	13.52	13.46
Fe_2O_3	4.62	4.60	4.88	4.79	4.21	4.49	4.52	4.51
MnO	0.13	0.14	0.16	0.16	0.14	0.15	0.15	0.15
MgO	0.23	0.25	0.21	0.26	0.23	0.21	0.23	0.21
CaO	1.53	1.37	1.52	1.49	1.36	1.39	1.44	1.38
Na_2O	5.22	5.04	5.48	5.41	4.86	5.48	5.48	5.59
K_2O	3.27	3.52	3.31	3.48	3.30	3.48	3.47	3.51
P_2O_5	0.08	0.05	0.05	0.06	0.05	0.04	0.05	0.04
LOI	2.81	2.93	0.26	0.07	3.43	0.15	0.15	0.21
Total	99.47	99.46	99.39	99.71	99.49	99.17	99.72	100.28
Trace elements (XRF, ppm)								
Rb	75	78	77	82	76	81	79	
Sr	167	120	165	155	121	125	133	
Y	93	97	96	99	94	99	97	
Zr	881	839	920	935	907	940	928	
Nb	116	118	119	120	117	121	119	
Ba	652	654	638	680	650	676	669	
Trace elements (ICPMS, ppm)								
Li	19	22	22	21	25	25	24	24
B	3		12					
Sc	4		5		4			
Ti	2,011	2,053	2,164	2,135	2,101	1,692	1,814	1,612
V	3	9	1	1	4	1	1	1
Cr	0	1	1	11	2	3	3	0
Co	1	3	1	1	1	1	1	1
Ni	0	1	0	0	1	0	0	0
Cu	3	7	4	4	4	6	5	6
Zn	184	184	189	183	173	178	176	175
Rb	74	59	79	78	82	78	75	76
Sr	162	121	169	161	129	133	137	122
Y	89	96	96	100	96	101	97	97

Table 1 (continued)

Sampling area	4	4	4	4	5	5	5	5
Locality	Austurgil	Austurgil	Gvendarfell	Austurgil	Near Huldufjöll 1 (IMNH)	Kriki	Near Huldufjöll 2 (IMNH)	Huldufjöll 3 (IMNH)
Locality No.	38 (URI-95)	37 (URI-95)	97 (URI-95)	36 (URI-95)		87 (URI-95)		
Sample No.	IC95-75	IC95-65	IC95-142	IC95-60	KAT01-A	IC95-132	KAT01-B	KAT04
Exposure	Interbed layer	Interbed layer	Columnar lava	Interbed breccia	Nunatak	Scree	Nunatak	Nunatak
Rock	Tephra	Tephra	Obsidian	Obsidian	Pumice	Obsidian	Obsidian	Obsidian
Zr	717	726	814	949	937	964	932	933
Nb	119	132	127	137	126	139	133	134
Mo	5		6		6			
Sn	7		7		10			
Sb	0	0	0	0	0	0	0	0
Cs	1	1	1	1	1	1	1	1
Ba	622	602	669	650	672	652	638	632
La	80	88	85	91	94	91	88	89
Ce	177	183	187	188	190	189	183	184
Pr	23	23	24	24	24	24	23	23
Nd	80	88	84	92	92	91	89	89
Sm	18	19	19	20	19	20	19	19
Eu	4	4	4	4	4	4	4	4
Gd	17	18	18	18	18	18	18	18
Tb	3	3	3	3	3	3	3	3
Dy	15	16	16	17	17	17	16	16
Ho	3	3	3	3	3	3	3	3
Er	8	9	9	9	9	9	9	9
Yb	8	8	8	8	8	8	8	8
Lu	1	1	1	1	1	1	1	1
Hf	18	18	20	22	22	22	22	22
Ta	7	8	8	8	8	8	8	8
Pb	7	7	7	7	8	7	7	9
Th	11	13	12	13	13	13	12	13
U	3	4	4	4	4	4	4	4
Isotopic ratios (TIMS)								
$^{87}Sr/^{86}Sr$			0.703456 (±7)			0.703411 (±7)	0.703439 (±2)	
$^{143}Nd/^{144}Nd$			0.512780 (±1)			0.512891 (±6)		

Table 1 (continued)

Sampling area	6	6	6	6	6	7
Locality	Bláfell	Enta	Bláfell	Enta	Austmannsb.	Álftaver
Locality No.	116 (URI-95)	20 (OU-02)	116 (URI-95)	20 (OU-02)	19 (OU-02)	17 (OU-02)
Sample No.	IC95-194	KAT02-19b	IC95-193	KAT02-19a	KAT02-18	KAT02-17
Exposure	Interbed layer	Nunatak	Lava flow	Nunatak	Nunatak	Lava flow
Rock	Tuff	Pumice	Obsidian	Obsidian	Rhyolite	Basalt
Major elements (XRF, wt%)						
SiO_2	48.62	68.70	70.04	70.54	71.24	47.16
TiO_2	3.72	0.30	0.35	0.29	0.34	4.46
Al_2O_3	13.34	13.07	13.26	13.36	13.90	13.10
Fe_2O_3	15.79	4.37	4.77	4.45	3.45	16.64
MnO	0.26	0.14	0.15	0.15	0.07	0.22
MgO	4.15	0.18	0.16	0.15	0.09	4.96
CaO	8.45	1.33	1.42	1.33	1.03	9.61
Na_2O	3.31	5.28	5.34	5.48	5.55	2.86
K_2O	0.98	3.39	3.57	3.49	3.74	0.76
P_2O_5	0.85	0.04	0.04	0.04	0.04	0.53
LOI	−0.05	3.04	0.09	0.31	0.32	−0.26
Total	99.42	99.85	99.19	99.58	99.76	100.03
Trace elements (XRF, ppm)						
Rb	18	79	86	82	85	16
Sr	518	114	135	117	117	439
Y	49	97	101	99	77	44
Zr	302	909	960	942	767	258
Nb	42	118	122	122	112	36
Ba	274	670	700	689	708	234
Trace elements (ICPMS, ppm)						
Li	7	23	22	24	14	5
B	15	15		7		9
Sc	6	6		7	2	23
Ti	22,473	1,826	2,089	1,760	1,961	28,273
V	219	4	1	1	2	428
Cr	1	3	86	4	2	8
Co	34	1	1	1	2	49
Ni	3	1	2	0	1	21
Cu	15	13	6	5	6	59
Zn	158	189	187	178	150	155
Rb	19	79	83	83	82	13
Sr	538	119	144	114	116	425
Y	50	91	105	96	71	40

Table 1 (continued)

Sampling area	6	6	6	6	6	7
Locality	Bláfell	Enta	Bláfell	Enta	Austmannsb.	Álftaver
Locality No.	116 (URI-95)	20 (OU-02)	116 (URI-95)	20 (OU-02)	19 (OU-02)	17 (OU-02)
Sample No.	IC95-194	KAT02-19b	IC95-193	KAT02-19a	KAT02-18	KAT02-17
Exposure	Interbed layer	Nunatak	Lava flow	Nunatak	Nunatak	Lava flow
Rock	Tuff	Pumice	Obsidian	Obsidian	Rhyolite	Basalt
Zr	300	950	992	967	437	261
Nb	47	130	143	133	117	37
Mo		6		6	4	2
Sn		8		8	9	2
Sb	0	0	0	0	0	0
Cs	0	1	1	1	1	0
Ba	246	685	684	671	684	187
La	35	77	96	86	78	26
Ce	80	173	200	192	173	64
Pr	11	22	25	24	22	9
Nd	50	80	96	85	81	36
Sm	12	18	21	19	17	9
Eu	4	4	4	4	3	3
Gd	12	18	19	18	15	10
Tb	2	3	3	3	2	1
Dy	9	16	18	16	13	8
Ho	2	3	4	3	3	1
Er	5	9	10	9	7	4
Yb	3	8	9	8	6	3
Lu	0	1	1	1	1	0
Hf	7	23	23	23	12	6
Ta	3	8	8	8	7	2
Pb	2	8	8	8	10	5
Th	3	11	14	12	13	2
U	1	4	4	4	3	1
Isotopic ratios (TIMS)						
$^{87}Sr/^{86}Sr$	0.703399 (±2)	0.703479 (±13)	0.703398 (±5)	0.703392 (±3)		0.703347 (±3)
$^{143}Nd/^{144}Nd$	0.512780 (±2)	0.512954 (±3)	0.512791 (±20)	0.512880 (±6)		0.512959 (±4)

PFD pyroclastic flow deposit; *LOI* loss on ignition

Sample KAT02-17 from the Eldgjá flood lava, AD 934–940 years. Large difference in Zr values between the analytical methods due to incomplete dissolution (ICPMS) of zircon crystals

Iceland-Norwegian seas, the Faeroe Islands, part of the British Isles, S Scandinavia, and W Russia (e.g. Wastergard et al. 2000). The products of this major eruption, estimated to be at least 6–7 km^3 in volume, represent the youngest rhyolitic melt that was erupted from the caldera. Its composition is peralkaline (Na_2O+K_2O=9.2–9.7 wt% for SiO_2=71.1–71.6 wt%). Prior to this major silicic eruption, only a few late Pleistocene basaltic eruptions are known and dated in deep-sea tephra layers (Lacasse et al. 1998). They display the high-Ti glass composition characteristic of Katla (TiO_2=4.0–4.4 wt% for MgO=4.6–5.6 wt%).

Rock sampling and analytical methods

Rock sampling

During two field expeditions conducted in 1995 (University of Rhode Island, USA) and 2002 (Open University, UK), several areas were visited and sampled (Fig. 1). These areas cover part of the Mýrdalsjökull ice cap and the unglaciated land southward to the coast. Exposures of lavas, pyroclastic rocks, and jökulhlaup deposits form the basis of this study. They include (1) basaltic lava flows (e.g. Eldgjá lavas, AD 934–940) and hyaloclastite sequences of historical to late Pleistocene age south and southeast of the caldera, (2) ice-free rhyolitic lava sequences of middle to late Pleistocene age along the Mýrdalsjökull ice margin at Bláfell, Gvendarfell, Kriki (localities 6B, 4B, and 5B; Fig. 2), and at a nunatak at Austmannsbunga (locality 6A;

Fig. 2), (3) exposures of pyroclastic rocks from the last major silicic explosive eruption, about 11,980 years BP, on nunataks at Enta and above Huldufjöll (localities 6C and 5A; Fig. 2), at the southern ice margin at Vesturgil (locality 4C; Fig. 2), and down slope at Dalárgil, Hofsárgil, Húsárgil, Rjúpnagil, Sólheimar (localities 1A-D; Fig. 2), (4) layers of historical (e.g. Katla 1918) and prehistorical tephra falls (e.g. SILK tephras, ~1,700 to ~6,600 ^{14}C years BP, after Larsen et al. 2001), and jökulhlaups deposited south of the caldera and along the shoreline at Skógasandur, Sólheimasandur, Dyrhólaey, Mýrdalssandur (Fig. 2).

XRF and ICPMS whole-rock analyses

Seventy-nine whole-rock samples were selected for major and trace element analysis by X-ray fluorescence (XRF) at the Open University, using an ARL 8420+ dual goniometer wavelength-dispersive XRF spectrometer. Concentrations of major and minor elements (Si, Ti, Al, Fe, Mn, Mg, Ca, Na, K, P) were determined on glass discs, produced by melting 1 part rock powder (dried at 110°C) with five parts of dried lithium metaborate/tetraborate flux (Johnson Matthey Spectroflux 100B) in Pt-5%Au crucibles at 1,100°C for 15–20 min. Loss on ignition (LOI) that accounts for volatile constituents (e.g. H_2O, CO_2) was determined by igniting dried rock powders in alumina crucibles at 800°C for about 1 h and then calculating the percentage weight loss. Concentrations of selected trace elements (Rb, Sr, Y, Zr, Nb, Ba, Pb, Th, U, Sc, V, Cr, Co,

Fig. 3 a–c Photomicrographs showing magma mingling in dacite (IC95-83, IC95-136A) and rhyolite (IC95-135), respectively. d Photomicrograph of flow-banded obsidian (IC95-36) including dark vesicular enclave (upper left) and euhedral olivine crystal (bottom right). e Photomicrograph of felsic xenolith (IC95-118) including interstitial glass, partly resorbed plagioclase, and disaggregated green amphibole surrounded by an oxide margin (centre). f Photomicrograph of felsic xenolith (IC95-69) showing granophyric texture under crossed polarised light. Area size of photomicrographs, 2×3 mm. Location, type, and whole-rock composition of rock specimens, see Table 1
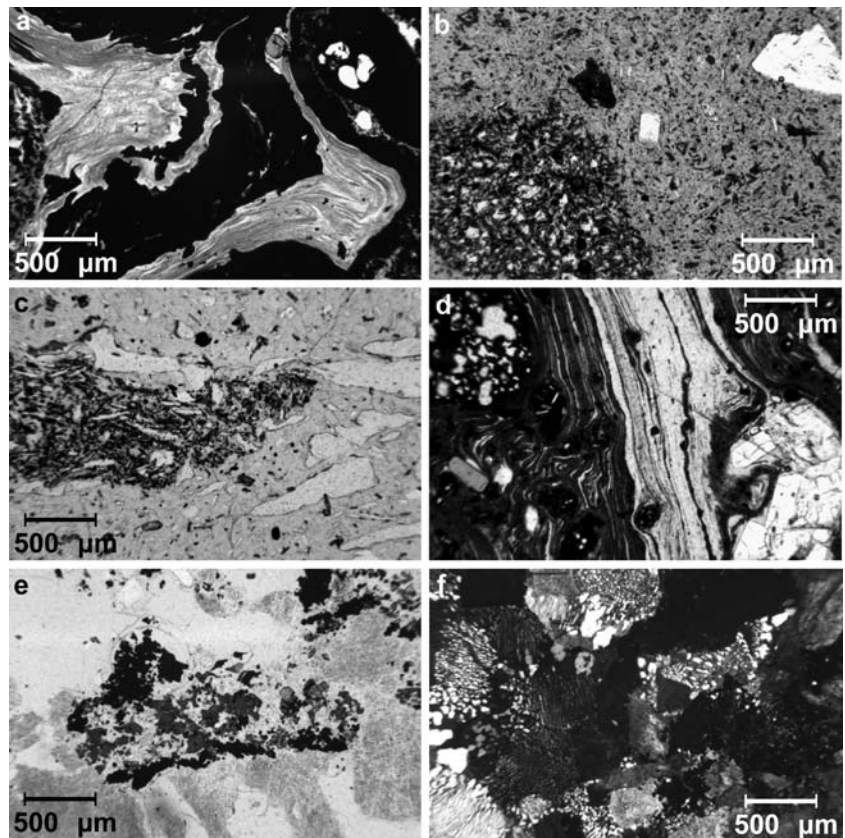
Ni, Cu, Zn, Ga, Mo, As, S) were measured on pressed powder pellets that were produced by thoroughly mixing rock powder (~10 mg) with 0.9 ml of polyvinylpyrollidone (PVP)/methyl cellulose binder (Watson 1996). Dolerite WS-E (Govindaraju et al. 1994) and microgranite OUG94 (Thompson et al. 1996) were analysed as internal standards to monitor the accuracy of major element data. The USGS international reference materials basalt BHVO-1, quartz latite QLO-1, diabases DNC-1 and W-2 were used to monitor the accuracy of trace element data, using recommended values obtained from Potts et al. (1992).

Thirty-eight whole-rock samples were selected for analysis of the concentration of 38 trace elements, including REE, by Inductively Coupled Plasma Mass Spectrometry using an Agilent 7500 ICPMS instrument at the Open University. The dissolution procedure was a standard $HF-HNO_3$ digestion (e.g. Eggins et al. 1997). Calibration was based on up to six reference materials (BCR1, BIR1, AC, RGM1, BHVO1-2 and AGV1) using recommended element concentrations.

Isotopic techniques

Sr and Nd were separated using standard ion exchange techniques and Sr and Nd isotopes were determined on a Finnigan Triton (TIMS) at the Open University. Sr was fractionation-corrected to $^{86}Sr/^{88}Sr=0.1194$ and $^{142}Nd/^{144}Nd=0.7219$. NBS 987=0.710235 (±0.000009) on 25 analyses and Johnson and Matthey Nd=0.511822 (±0.000002) on 20 analyses. Quote errors are two-standard deviations. This external precision is comparable with Thirlwall et al. (2004) and is better than most of other published Nd data on Iceland, where a typical two-standard deviation is 0.000020, and hence allows us to observe tight correlations between Nd and other parameters.

EMP analysis of volcanic glass

Volcanic glass from tephras and pyroclastic rocks was analysed with two different electron microprobes, a Cameca Camebax (Brown University) and a Cameca SX100 (Open University). Sodium loss in silicic glasses (i.e. with SiO_2 >60 wt%) was minimised at the Brown microprobe by using a beam defocused to 10 μm and a

Fig. 4 Variation diagrams of XRF whole-rock compositions for Na_2O+K_2O, TiO_2, Al_2O_3, Fe_2O_3, CaO and MgO (wt%) vs. SiO_2 (wt%). *Numbers in brackets* refer to sampling areas (see Fig. 1)
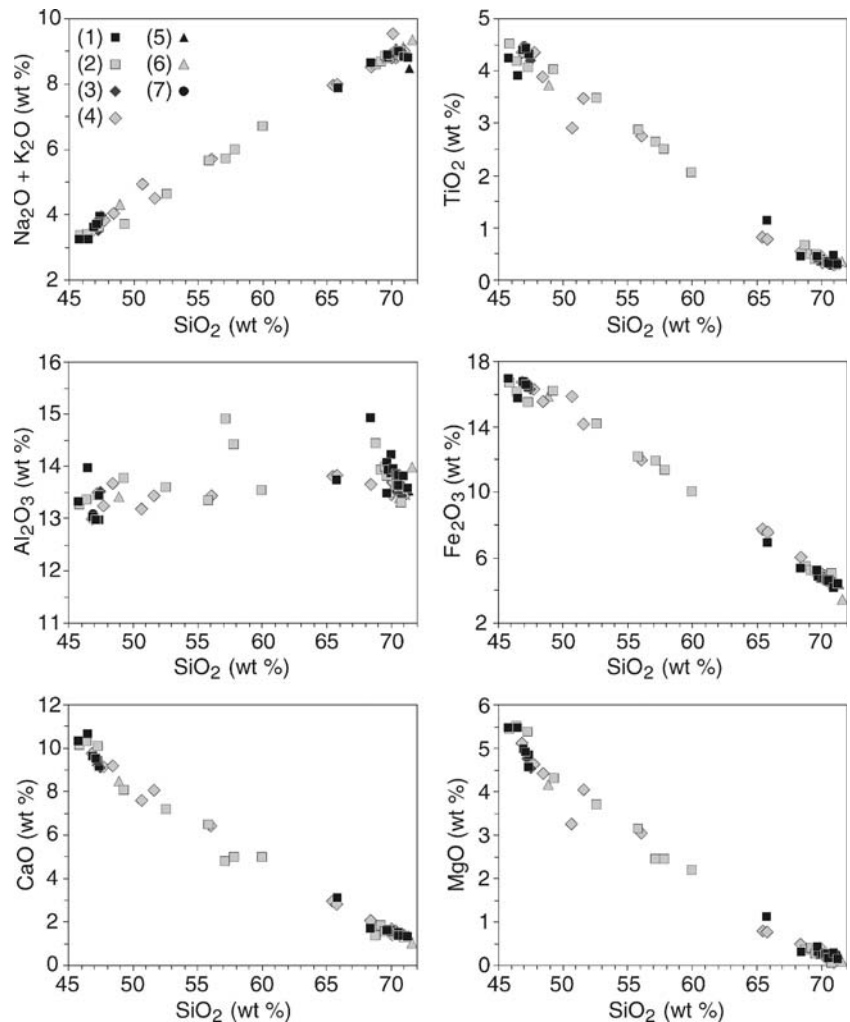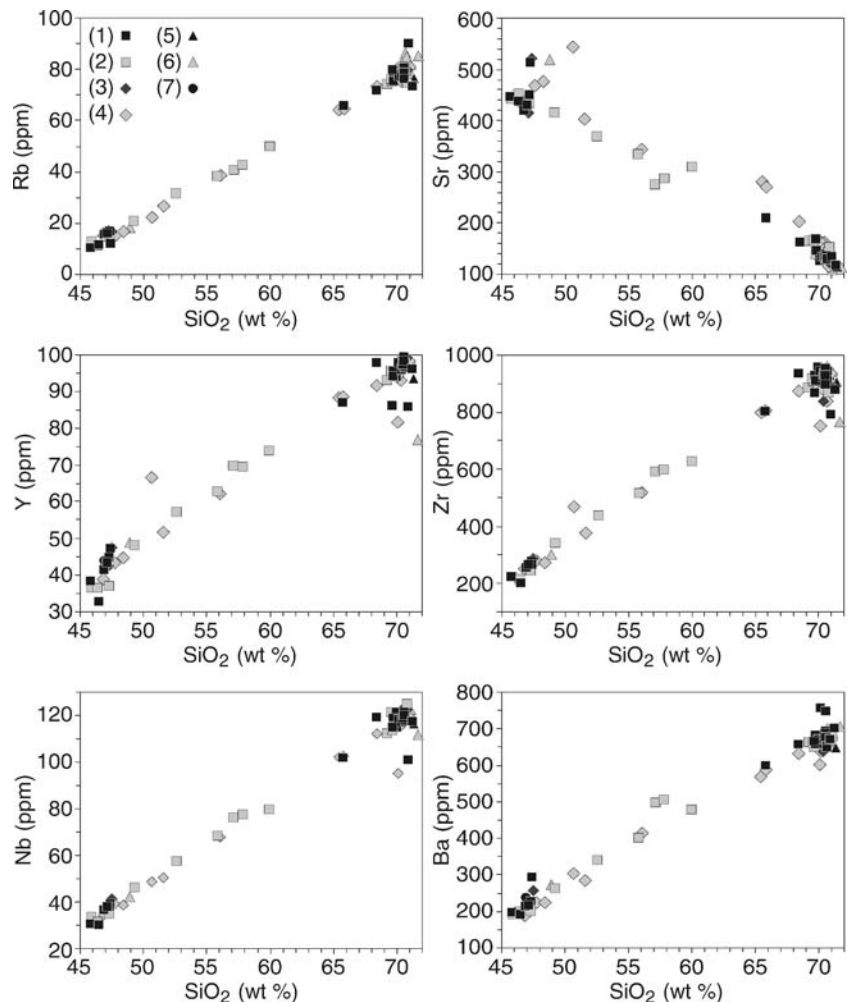
Fig. 5 Variation diagrams of XRF whole-rock compositions for Rb, Sr, Y, Zr, Nb, and Ba (ppm) vs. SiO$_2$ (wt%). *Numbers in brackets* refer to sampling areas (see Fig. 1)

routine collecting counts at regular intervals (2 s) and extrapolating the Na-decay curve back to count initiation (Nielsen and Sigurdsson 1981), and at the OU microprobe by using a rastered beam scanning an area of ~15×20 μm. A 10-nA-beam current was used with an accelerating voltage of either 15 kV (Brown) or 20 kV (OU). The same correction method was applied to all glass analyses in order to minimise the effects of the different microprobe operating conditions. International reference glass materials (VG2, KN18) were systematically analysed before and after each unknown glass sample. Oxide weight percents (e.g. SiO$_2$, Al$_2$O$_3$) of the unknown glass samples were corrected from the deviation estimated between the analysed and recommended compositions of either VG2 for basaltic glasses or KN18 for silicic glasses. By considering this correction method after minimisation of Na-loss, the reproducibility of glass analyses between the two microprobes was remarkable, with similarity coefficients >97% (based on SiO$_2$, Al$_2$O$_3$, FeO, CaO, Na$_2$O, and K$_2$O) for tested rhyolitic glasses that are the most susceptible to volatilisation (e.g. Na-loss). The range of major element concentrations was found to be relatively narrow in all of the basaltic, dacitic, or rhyolitic glass samples. Averaged composition and standard deviation were calculated from about 10 to 20 individually analysed points (e.g. single

glass shards, matrix glass of pumice, obsidian glass). Glassy samples with a large amount of microlites were ignored. The few samples displaying a large compositional range were subdivided into several geochemical affinities prior to averaging.

Petrography of lavas and pyroclasts

The Katla rock suite of this study consists dominantly of Fe-Ti transitional alkali basalts and mildly alkalic rhyolites. In addition, there are rare volcanic rock specimens of intermediate composition that appear to be mixed magmas in origin (Table 1; Figs. 3, 4 and 5). The terminology used here for the extrusive volcanic rocks is based on their normalised XRF whole-rock composition and total alkali-silica classification (Le Bas et al. 1986).

Basalts

Basaltic lavas (SiO$_2$ ~45–52 wt%; Table 1, Figs. 4 and 5) erupted from Katla have a relatively uniform petrography. The groundmass is mainly microcrystalline with few macrophenocrysts (<1%) of plagioclase feldspar, olivine

and clinopyroxene (augite). The macrophenocrysts are subhedral to euhedral, up to a few millimetres in size, with the plagioclase being moderately zoned and the clinopyroxene occasionally resorbed. The micropheno-crysts consist of lath-shaped plagioclase showing preferential orientation indicative of the flowage. Occasional glomerocrysts of plagioclase, clinopyroxene, olivine and iron oxides are formed as a result of near simultaneous crystallisation of these phases. Details on the petrography and mineralogy of Katla basalts are also given in Jakobsson (1979). Vesicularity of spatter-like samples can amount to about 50%. Basaltic lapilli (>2 mm size) and medium to coarse ash (~0.5–2 mm size) from glacier flood (jökulhlaup) deposits and tephra fall deposits consist of juvenile grains of brownish glass that include sub-rounded vesicles less than ~1–2 mm size. Pipe-shaped vesicles are also present. The vesicularity of the lapilli varies from less than 30 to about 50%. The microphenocrysts mainly consist of small needle-like plagioclase crystals up to a few hundred microns in size, with rare sub-rounded clinopyroxene. Excessive amounts of microlites often make basaltic lapilli opaque in thin section and unsuitable for electron micro-probe analysis of the glass. Fine to medium basaltic ash (0.12–1 mm size) consists of sideromelane (brownish glass) and tachylite (opaque microcrystalline) grains, approximately in equal amounts and identical in texture to lapilli. The vesicularity of sideromelane grains generally decreases when they are associated with hyaloclastites, with the glass often showing cracks resulting from rapid cooling (quenching).

Basaltic andesites, andesites, dacites

The few rock and pyroclast (tephra) samples of intermediate bulk composition, i.e. from basaltic andesite to dacite (SiO$_2$ ~55–66 wt%; Table 1, Figs. 4 and 5), fall into three petrographic categories. The first category consists of a few hard-rock specimens, e.g. IC95-85 and IC95-83 (sampling area 2; Table 1), of basaltic-andesite to andesite composition (SiO$_2$ ~55–60 wt%). They show complex texture with two main components that are mixed: a clear colourless silicic glassy component, typically devitrified, and an opaque (mafic) vesicular component. Two samples (scoria, volcanic bomb) were found embedded in a massive flood deposit in Holt (locality 2B; Fig. 2). Both show the same mixed texture of opaque vesicular clasts, up to ~1–2 cm size, and a few colourless glassy clasts that are partly devitrified. The clasts, of distinct bimodal composition, are mainly elongated and in a medium to coarse-grained matrix consisting of colourless glass and opaque fragments. The matrix also contains macrophenocrysts of sub-rounded plagioclase and subhedral to euhedral olivine crystals. The olivine crystals, up to ~1–2 mm size, are moderately zoned and include small oxides. The opaque vesicular clasts contain a few small inclusions of plagioclase and olivine. The two mafic and silicic components are occasionally more imbricated and show evidence of plastic deformation

and flow structure clearly indicative of magma mingling (Fig. 3a).

The second category of erupted products of basaltic andesite composition (SiO$_2$ ~55–60 wt%) is represented by mixed tephra, e.g. IC95-92 (sampling area 2). The coarse tephra is poorly sorted and occurs in a distal flood (jökulhlaup) deposit in Dyrhólaey (locality 2A; Fig. 2). Its composition is bimodal, with two main components of approximately equal proportions. The first component consists of colourless glass shards (cuspate-shaped, bubble walls) and a few grains of pumice, whereas the second component consists of juvenile brownish glassy (side-romelane) grains and opaque microcrystalline (tachylite) grains. Sideromelane and tachylite grains are dominantly vesicular. Basaltic lithic grains are also present. Electron microprobe analysis of the brownish and colourless glassy components confirms a distinct bimodal basaltic and rhyolitic composition (Table 2).

The third category of intermediate rocks is represented by a few pyroclastic samples of dacite composition (SiO$_2$ ~65–66 wt%), including an obsidian, KAT02-38b (sampling area 1), found in W. Húsárgil (locality 1C; Fig. 2). Its agglutinate texture suggests accumulation and compaction (welding) of hot glassy pyroclasts, including colourless glassy clasts and opaque clasts up to ~0.5–1 cm size. The opaque variety is mainly vesicular with microphenocrysts of plagioclase and clinopyroxene. The matrix consists of welded and devitrified glass shards, with macropheno-crysts of plagioclase that can be significantly resorbed. Two other rock specimens (obsidian, pumice) with the same narrow dacitic composition (SiO$_2$ ~65–66 wt%), IC95-136A and IC95-136B (sampling area 4; Table 1), were found in a pyroclastic flow deposit in Vesturgil (locality 4C; Fig. 2). The obsidian consists of a microcrystalline groundmass of thin plagioclase needles and a few oxides. Macrophenocrysts include a few percent of euhedral and partly resorbed plagioclase, euhedral olivine and very few greenish clinopyroxenes. Sub-rounded enclaves (<2–3 mm size) of more mafic texture are enclosed in the matrix (Fig. 3b). The pumice from the same pyroclastic deposit is highly vesicular (~60%) and contains less than 1% of macrophenocrysts and some microlites in the matrix glass.

Rhyolites

The extrusive rocks of rhyolitic bulk composition (SiO$_2$ ~68–72 wt%; Table 1, Figs. 4 and 5) fall into three main petrographic groups that are exposed along and near the rim of the Katla subglacial caldera (Fig. 2). The first group consists primarily of pumices in pyroclastic flow deposits that are exposed on either side of the Sólheimajökull glacier, along several gullies in Dalárgil, Hofsárgil, Húsárgil, and Rjúpnagil (localities 1A-D; Fig. 2), and, secondly, of proximal fall deposits on nunataks in Enta and above Huldufjöll (localities 6C and 5A; Fig. 2). The pumice clasts are generally flattened when incorporated in pyroclastic flow units, e.g. KAT02-12b (sampling area 1;

Table 2 Selected glass analyses of volcanic rocks from the Katla subglacial caldera

Sampling area	1	1	1	1	1	1	1	1	1	1	1	2
Locality	E. Dalárgil	W. Hofsárgil	E. Rjúpnagil	W. Húsargil	E. Dalárgil	E. Rjúpnagil	E. Rjúpnagil	E. Rjúpnagil	E. Dalárgil	Vestasthháls	Sjónarhóll	Dyrhólaey
Locality No.	8 (OU-02)	11 (OU-02)	23 (OU-02)	30 (OU-02)	8 (OU-02)	23 (OU-02)	22 (OU-02)	23 (OU-02)	8 (OU-02)	19 (URI-95)	2 (URI-95)	61 (URI-95)
Sample No.	KAT02-9b	KAT02-12b	KAT02-27b	KAT02-39	KAT02-10	KAT02-26	KAT02-25	KAT02-27a	KAT02-9a	IC95-32	IC95-06	IC95-92
Exposure	PFD	PFD	PFD	scree	PFD	PFD	Interbed layer	PFD	PFD	PFD	Scree	Flood deposit
Rock	Pumice	Pumice	Pumice	Pumice	Pumice	Pumice	Tephra	Obsidian	Bulk matrix	Obsidian	Xenolith	Mixed tephra
No. of analyses	8	6	17	17	14	17	16	15	14	8	10	13
SiO$_2$ (wt%)	68.36 (0.85)	68.85 (0.21)	70.15 (0.43)	70.20 (0.43)	70.51 (0.60)	70.72 (0.28)	70.80 (0.25)	70.87 (0.38)	71.30 (0.47)	71.38 (0.27)	75.50 (0.96)	48.34 (1.41)
TiO$_2$	0.27 (0.01)	0.27 (0.02)	0.27 (0.02)	0.28 (0.02)	0.27 (0.01)	0.28 (0.02)	0.29 (0.02)	0.29 (0.02)	0.28 (0.02)	0.31 (0.03)	0.42 (0.15)	4.70 (0.57)
Al$_2$O$_3$	13.09 (0.43)	12.82 (0.08)	13.19 (0.16)	13.16 (0.08)	13.24 (0.14)	13.26 (0.12)	13.27 (0.10)	13.36 (0.10)	13.61 (0.22)	13.33 (0.19)	11.50 (0.25)	13.18 (1.11)
FeO	3.57 (0.08)	3.62 (0.03)	3.83 (0.05)	3.83 (0.06)	3.81 (0.06)	3.84 (0.07)	3.82 (0.05)	3.86 (0.07)	3.86 (0.05)	3.82 (0.17)	2.14 (0.18)	14.88 (1.16)
MnO	0.14 (0.02)	0.13 (0.01)	0.15 (0.01)	0.14 (0.01)	0.14 (0.01)	0.15 (0.01)	0.14 (0.01)	0.14 (0.01)	0.14 (0.01)	0.11 (0.05)	0.14 (0.06)	0.20 (0.06)
MgO	0.18 (0.03)	0.19 (0.02)	0.20 (0.02)	0.20 (0.03)	0.20 (0.02)	0.20 (0.02)	0.20 (0.02)	0.20 (0.02)	0.20 (0.02)	0.21 (0.03)	0.22 (0.02)	4.71 (0.40)
CaO	1.33 (0.03)	1.28 (0.03)	1.34 (0.07)	1.26 (0.04)	1.37 (0.06)	1.29 (0.05)	1.27 (0.06)	1.27 (0.06)	1.28 (0.03)	1.37 (0.08)	0.66 (0.08)	9.78 (0.67)
Na$_2$O	5.76 (0.12)	5.72 (0.14)	5.66 (0.09)	5.63 (0.09)	5.69 (0.12)	5.79 (0.13)	5.73 (0.12)	5.77 (0.13)	5.81 (0.08)	5.92 (0.27)	4.68 (0.29)	3.08 (0.16)
K$_2$O	3.37 (0.05)	3.45 (0.05)	3.51 (0.05)	3.49 (0.04)	3.45 (0.05)	3.50 (0.04)	3.52 (0.05)	3.53 (0.05)	3.50 (0.08)	3.47 (0.08)	4.17 (0.11)	0.76 (0.25)
Total	96.08 (0.82)	96.33 (0.30)	98.30 (0.68)	98.19 (0.53)	98.68 (0.73)	99.04 (0.35)	99.05 (0.32)	99.30 (0.56)	99.99 (0.52)	99.93 (0.31)	99.42 (0.78)	100.36 (0.74)

Sampling area	2	2	2	2	2	2	2	2	2	3	3	3
Locality	Holt	Dyrhólaey	Oddnýjartjörn	Holt	Oddnýjartjörn	Holt	Steigarháls	Holt	Brekkur I	W. Múlakvísl	W. Múlakvísl	Lambaskörð
Locality No.	59 (URI-95)	61 (URI-95)	107 (URI-95)	59 (URI-95)	107 (URI-95)	59 (URI-95)	103 (URI-95)	59 (URI-95)	75 (URI-95)	43 (OU-02)	43 (OU-02)	66 (URI-95)
Sample No.	IC95-87	IC95-92	IC95-155	IC95-83	IC95-154	IC95-85	IC95-148	IC95-85	IC95-118	KAT02-64	KAT02-56	IC95-98
Exposure	Flood deposit	Flood deposit	Interbed layer	Flood deposit	Interbed layer	Flood deposit	Interbed layer	Flood deposit	Quarry pit	Interbed layer	Interbed layer	Interbed layer
Rock	Pumice	Mixed tephra	Tephra	Volcanic bomb	Tephra	scoria	Pumice	scoria	Granophyre	Tephra	Tephra	Scoria
No. of analyses	8	11	12	10	12	10	10	8	8	17	15	10
SiO$_2$ (wt%)	71.00 (0.72)	71.23 (0.73)	71.65 (0.83)	71.69 (0.29)	71.86 (1.03)	72.07 (0.94)	72.10 (0.59)	74.62 (0.86)	64.21 (0.60)	65.26 (0.69)	65.73 (0.38)	71.19 (0.69)
TiO$_2$	0.27 (0.03)	0.28 (0.06)	0.26 (0.06)	0.29 (0.05)	0.31 (0.04)	0.24 (0.03)	0.28 (0.04)	0.18 (0.05)	1.32 (0.06)	1.20 (0.04)	1.19 (0.04)	0.30 (0.06)
Al$_2$O$_3$	13.32 (0.18)	13.47 (0.13)	13.10 (0.43)	13.45 (0.13)	13.30 (0.42)	12.77 (0.27)	13.62 (0.29)	11.21 (0.30)	14.07 (0.66)	14.08 (0.24)	13.95 (0.08)	13.30 (0.15)
FeO	3.87 (0.21)	3.95 (0.11)	3.24 (0.21)	3.64 (0.20)	3.33 (0.13)	3.11 (0.08)	3.71 (0.44)	2.74 (0.29)	5.91 (0.23)	5.70 (0.09)	5.50 (0.08)	3.95 (0.23)
MnO	0.14 (0.02)	0.14 (0.04)	0.12 (0.04)	0.13 (0.05)	0.13 (0.04)	0.11 (0.06)	0.13 (0.06)	0.18 (0.05)	0.19 (0.01)	0.19 (0.01)	0.19 (0.01)	0.15 (0.06)
MgO	0.21 (0.02)	0.21 (0.02)	0.12 (0.03)	0.18 (0.03)	0.11 (0.02)	0.09 (0.02)	0.21 (0.03)	0.03 (0.02)	1.31 (0.07)	1.13 (0.03)	1.14 (0.05)	0.18 (0.07)
CaO	1.33 (0.07)	1.30 (0.04)	1.02 (0.12)	1.18 (0.09)	1.01 (0.06)	0.91 (0.07)	1.25 (0.15)	1.03 (0.08)	3.41 (0.27)	2.98 (0.04)	2.96 (0.05)	1.34 (0.14)
Na$_2$O	5.86 (0.10)	5.94 (0.23)	5.59 (0.38)	5.06 (0.25)	5.75 (0.31)	5.57 (0.27)	5.46 (0.25)	4.73 (0.18)	5.02 (0.26)	5.07 (0.14)	5.18 (0.15)	5.62 (0.27)
K$_2$O	3.52 (0.14)	3.48 (0.12)	3.63 (0.18)	3.89 (0.17)	3.62 (0.17)	3.79 (0.08)	3.08 (0.12)	4.08 (0.09)	2.51 (0.11)	2.67 (0.04)	2.70 (0.04)	3.51 (0.11)
Total	99.52 (1.15)	100.01 (0.81)	98.72 (1.45)	99.50 (0.25)	99.41 (1.38)	98.67 (1.40)	99.83 (0.44)	98.81 (0.74)	97.96 (0.72)	98.29 (0.89)	98.53 (0.52)	99.53 (0.42)

Sampling area	3	4	4	4	4	4	4	4	5	6	6
Locality	Thakgil	Austurgil	Austurgil	Austurgil	Austurgil	Austurgil	Vesturgil	Austurgil	near Huldufjöll	Enta	Enta
Locality No.	22 (URI-95)	37 (URI-95)	38 (URI-95)	37 (URI-95)	38 (URI-95)	37 (URI-95)	91 (URI-95)	37 (URI-95)	1 (IMNH)	20 (OU-02)	20 (OU-02)
Sample No.	IC95-37	IC95-67	IC95-74	IC95-68	IC95-75	IC95-66	IC95-136B	IC95-65	KAT01-A	KAT02-19b	KAT02-19a
Exposure	PFD	Interbed layer	Hayloclastite	Interbed layer	Interbed layer	Interbed layer	PFD	Interbed layer	Nunatak	Nunatak	Nunatak
Rock	Granophyre	Lapilli	Basalt	Bulk matrix	Tephra	Tuff	Pumice	Tephra	Pumice	Pumice	Obsidian
No. of analyses	8	13	12	12	15	10	9	15	9	12	15
SiO$_2$ (wt%)	74.06 (0.55)	47.25 (0.36)	48.14 (0.76)	48.56 (0.78)	71.07 (1.19)	48.97 (0.27)	70.23 (0.81)	71.23 (0.46)	70.19 (0.31)	69.11 (0.50)	71.36 (0.41)
TiO$_2$	0.30 (0.05)	4.60 (0.20)	4.17 (0.33)	4.17 (0.36)	0.26 (0.04)	4.30 (0.14)	0.44 (0.04)	0.20 (0.04)	0.28 (0.05)	0.27 (0.02)	0.26 (0.02)
Al$_2$O$_3$	12.07 (0.27)	13.24 (0.15)	13.51 (0.21)	13.53 (0.31)	13.10 (0.49)	13.42 (0.17)	13.35 (0.20)	12.99 (0.17)	12.72 (0.13)	13.13 (0.19)	13.44 (0.11)
FeO	2.68 (0.08)	15.45 (0.33)	14.58 (0.38)	14.55 (0.63)	3.26 (0.21)	14.41 (0.21)	4.15 (0.12)	3.42 (0.15)	3.72 (0.10)	3.69 (0.04)	3.91 (0.05)
MnO	0.15 (0.05)	0.23 (0.06)	0.20 (0.05)	0.23 (0.06)	0.12 (0.05)	0.25 (0.05)	0.17 (0.06)	0.14 (0.04)	0.15 (0.03)	0.14 (0.02)	0.14 (0.01)
MgO	0.20 (0.02)	5.07 (0.19)	4.77 (0.23)	4.74 (0.24)	0.12 (0.03)	4.54 (0.06)	0.26 (0.02)	0.08 (0.02)	0.18 (0.02)	0.14 (0.02)	0.14 (0.02)

Table 2 (continued)

Sampling area	3	4	4	4	4	4	4	4	5	6	6
Locality	Thakgil	Austurgil	Austurgil	Austurgil	Austurgil	Vesturgil	Austurgil	Austurgil	near Huldufjöll	Enta	Enta
Locality No.	22 (URI-95)	37 (URI-95)	38 (URI-95)	37 (URI-95)	37 (URI-95)	91 (URI-95)	38 (URI-95)	37 (URI-95)	1 (IMNH)	20 (OU-02)	20 (OU-02)
Sample No.	IC95-37	IC95-67	IC95-74	IC95-68	IC95-66	IC95-136B	IC95-75	IC95-65	KAT01-A	KAT02-19b	KAT02-19a
Exposure	PFD	Interbed layer	Hayloclastite	Interbed layer	Interbed layer	PFD	Interbed layer	Interbed layer	Nunatak	Nunatak	Nunatak
Rock	Granophyre	Lapilli	Basalt	Bulk matrix	Tuff	Pumice	Tephra	Tephra	Pumice	Pumice	Obsidian
Na_2O	5.37 (0.18)	2.92 (0.10)	3.17 (0.19)	3.13 (0.12)	3.21 (0.06)	5.67 (0.17)	5.65 (0.34)	5.55 (0.28)	5.28 (0.16)	5.88 (0.22)	5.72 (0.13)
K_2O	3.99 (0.10)	0.67 (0.07)	0.79 (0.08)	0.74 (0.20)	0.81 (0.05)	3.35 (0.11)	3.63 (0.15)	3.55 (0.08)	3.47 (0.10)	3.46 (0.06)	3.47 (0.04)
Total	99.68 (0.37)	100.29 (0.71)	99.71 (0.58)	100.08 (0.37)	100.00 (0.42)	99.15 (1.23)	98.18 (1.75)	98.22 (0.68)	97.13 (.)	97.05 (0.59)	99.69 (0.45)

KAT02-56, KAT02-59, KAT02-64, silicic tephras SILK-LN (3139±40 years 14C BP), SILK-MN (2975±12 years 14C BP), SILK-UN (2660±50 years 14C BP; Larsen et al. 2001). Mean and standard deviation of the mean in brackets

Table 1), and range from a few centimetres to about ~20 cm in size. They are highly vesicular (~60%) and present the same texture and mineralogy as the specimens of dacitic composition that were described earlier. Plagioclase macrophenocrysts (<1%) in the glassy matrix sometimes show signs of resorption, e.g. in pumices (KAT02-19b) from the Enta nunatak (locality 6C; Fig. 2).

The second petrographic group of rhyolitic rocks are mainly lavas exposed along the caldera rim, occasionally showing columnar jointing, e.g. at Gvendarfell (locality 4B; Fig. 2). They exhibit various stages of crystallisation, from obsidian to microcrystalline rhyolite, and their vesicularity varies from 0 to 30%. Obsidian clasts from a pyroclastic flow in Thakgil, IC95-36 (sampling area 3), show flow-banded texture, with bands of colourless glass with very few microlites (<5%) alternating with dark devitrified bands that include opaque vesicular clasts (<2 mm) with evidence of plastic or flow deformation (Fig. 3d). Macrophenocrysts of plagioclase (up to ~3–4 mm) and microphenocrysts of olivine and clinopyroxene are enclosed in the dark devitrified bands, whereas the clear glassy bands include microglomerocrysts of plagioclase, clinopyroxene, and oxide. Obsidians can acquire a pillow-like shape, e.g. IC95-135 in Vondhöfud (sampling area 4). The groundmass of this obsidian is microcrystalline with ~30–40% of microlites, moderately vesicular (~20%), and contains isolated euhedral macrophenocrysts of plagioclase (~2–3 mm size) or glomerocrysts when associated with oxides. Brownish enclaves, up to ~2 cm size, are enclosed in the matrix and show a microcrystalline and vesicular texture. They are often elongated parallel to the main stretching orientation as the vesicles (Fig. 3c). In addition to large pumices, pyroclasts of flow-banded obsidian, KAT02-19a (sampling area 6; Table 1), were also found on Enta nunatak (locality 6C; Fig. 2). Apart from the absence of dark enclaves, they show the same flow-banded texture as described before, with assemblages of plagioclase microphenocrysts concentrated in the dark devitrified bands and surrounded by a texture showing plastic or flow deformation. Obsidian clasts, KAT01-B (sampling area 5; Table 1), found on another nunatak above Huldufjöll (locality 5A; Fig. 2) contain ~20–30% of microlites and a microphenocryst assemblage of plagioclase, clinopyroxene, olivine, and oxide. The same petrographic group also includes a series of rhyolitic lavas with their groundmass microlite content (needle-like plagioclase crystals) ranging from ~40 to ~70%. These rhyolites, e.g. IC95-60, IC95-142, and IC95-132 (sampling areas 4 and 5; Table 1), are exposed at Gvendarfell, Austurgil, and Kriki (localities 4B, 4A, and 5B; Fig. 2), respectively. They are vesicle-free and contain macrophenocrysts of plagioclase (e.g. up to 3 mm size in IC95-60), clinopyroxene, and olivine (e.g. oxidised fayalite in IC95-60). Euhedral microphenocrysts of olivine enclosed in a flow-banded texture occasionally can be observed in specimen from Bláfell (locality 6B; Fig. 2), e.g. IC95-193 (sampling area 6; Table 1).

The third group of rocks of rhyolitic composition is represented by a crystal-rich lava exposed at a nunatak in

Austmannsbunga (locality 6A; Fig. 2). The rock (KAT02-18, sampling area 6; Table 1) is the most porphyritic and silicic (SiO$_2$ ~71–72 wt%) of all rhyolitic lavas that were studied. It contains large macrophenocrysts of partly resorbed plagioclase (up to ~5–6 mm size), greenish clinopyroxene, and olivine. The macrophenocrysts represent ~20–30% and are enclosed in a devitrified glassy matrix that contains a few glomerocrysts of plagioclase and oxide.

Leucocratic xenoliths

Leucocratic (felsic) xenoliths (felsite, granophyre) of pale-grey colour were found either embedded in pyroclastic flow deposits, or as loose blocks in screes. They mainly present a granular texture and their bulk SiO$_2$ content varies from 69 to 71 wt% (Table 1). They are characterised by various stages of partial melting with <5 to ~70% interstitial glass of rhyolitic composition (e.g. IC95-06, IC95-37, IC95-118; Table 2). One xenolith (KAT02-38a) was found encased in an obsidian block in W. Húsargil (locality 1C; Fig. 2). This xenolith includes crystals of plagioclase (<1–2 mm size), green pyroxene, and interstitial quartz that are moderately to extensively resorbed, in a

fine-grained matrix showing an early stage of disaggregating and partial melting. Some resorbed plagioclase crystals, probably derived from the xenolith, are incorporated in the host obsidian near the contact margin. Another xenolith (KAT02-37a) from the same area contains large subhedral crystals of plagioclase (~2–3 mm size) and sub-rounded quartz that are partially melted. Lath-shaped crystals (up to ~5 mm size) of green amphibole in the same specimen are almost entirely disaggregated and surrounded or replaced by patches of opaque Fe-Ti oxides. A more advanced stage of partial melting with ~60 and ~70% glass was found in two specimens, IC95-06 and IC95-37, in pyroclastic flow deposits in Sjónarholl (sampling area 1; Table 1) and in Thakgil (sampling area 3; Table 1), respectively. The first specimen (IC95-06) includes large resorbed plagioclase crystals, up to ~2–3 mm size, and patches of Fe-Ti oxides associated with the remnants of colourless pyroxene crystals. Another xenolith (IC95-05) collected in the same area differs in texture by having vesicles (up to ~10%) in the interstitial glass. The coarsest (IC95-118) of all xenoliths was found in a quarry in Brekkur I (sampling area 2). It is partly melted (~40% glass) and includes plagioclase crystals up to ~5 mm size, disaggregated crystals of amphibole showing pleochroism and surrounded by an opaque margin, and a few isolated subhedral

Fig. 6 Multi-element spider diagrams of ICPMS whole-rock compositions of trace elements normalised to N-MORB and C1 chondrite values from Sun and McDonough (1989). Mobile elements (Sr, K*, Rb, Ba) and immobile elements (Ta, Nb, Ce, Nb, Ce, P*, Zr, Hf, Sm, Ti, Y, Yb) ordered according to Pearce (1983). K*, P*: XRF whole-rock analyses. (Pm), (Tm): rare earth elements not analysed. SiO$_2$ (wt%) compositional range of whole rock (XRF normalised)
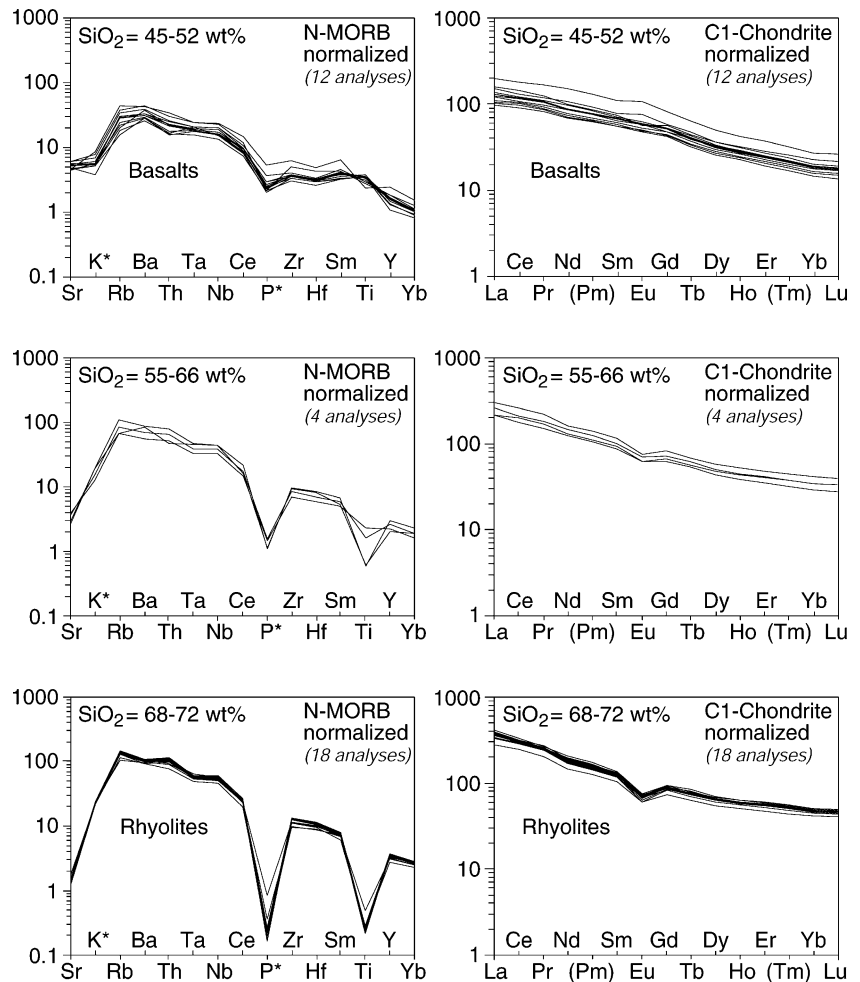
Fig. 7 Variation diagrams of ICPMS whole-rock compositions for **a** Ba vs. Sr, **b** Rb vs. Sr, **c** Sm/Nd vs. La/Yb, and **d** Dy/Yb vs. La/Yb. *Dashed lines* show the general differentiation trends in basalts and rhyolites. *Numbers in brackets* refer to sampling areas (see Fig. 1)
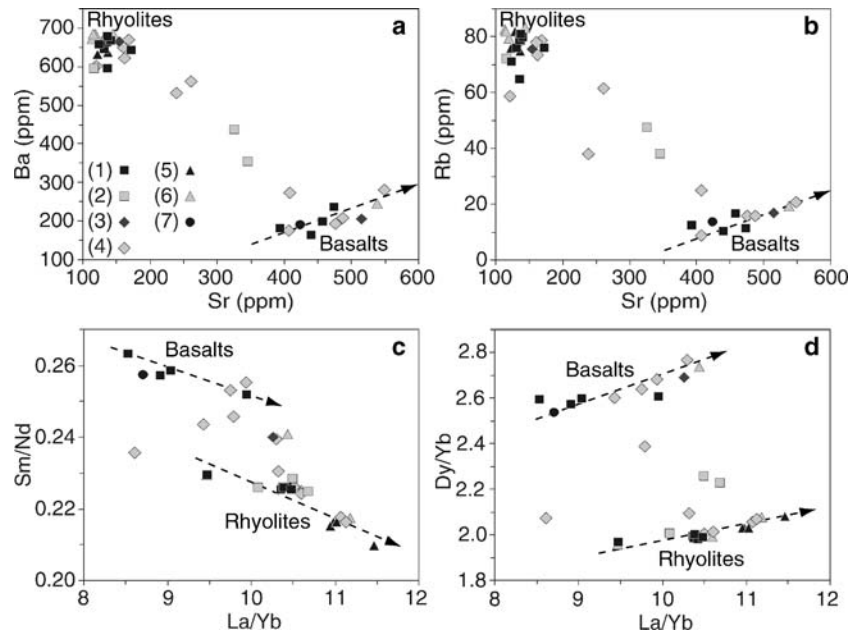
zircon crystals (Fig. 3e). A xenolith, IC95-69, from Austurgil (locality 4A; Fig. 2), exhibits typical granophyric texture showing with intimate intergrowth of quartz and feldspar (Fig. 3f).

Whole-rock geochemistry

Compositional range of major and trace elements

Major and trace element concentrations of whole rocks are listed in Table 1. All sampling areas show a common compositional trend between two end-members represented by Fe-Ti transitional-alkali basalts (SiO_2=45.0–52.5 wt%) and mildly alkalic rhyolites (SiO_2 >69.0 wt%; Figs. 4 and 5). Basaltic pyroclasts and lavas exposed down-slope from the caldera (e.g. in area 1 at Rjúpnagil and Skógasandur) or erupted from the Eldgjá fissure (e.g. in area 7, at Álftaver) are characterised, with very few exceptions, by TiO_2 (3.4–4.5 wt%), Fe_2O_3=14.0–17.0 wt%, CaO=7.6–10.7 wt%, MgO=4.1–5.6 wt%, Na_2O+K_2O=3.2–4.5 wt%, and Rb=10–30 ppm, Zr=200–380 ppm, Nb=30–50 ppm, Ba=180–310 ppm (Figs. 4 and 5). Volcanic rocks of rhyolitic composition which originated from the caldera, exposed as pyroclastic flow deposits down slope at Dalárgil, Hofsárgil, Húsárgil, and Rjúpnagil (localities 1A-D; Fig. 2), proximal pyroclastic fall deposits above Huldufjöll and at Enta (localities 5A and 6C; Fig. 2), and lavas at Gvendarfell, Kriki, Austmannsbunga, and Bláfell (localities 4B, 5B, 6A, and 6B; Fig. 2), also show a narrow compositional range, with TiO_2<0.7 wt%, Fe_2O_3=4.0–6.0 wt%, CaO<2.1 wt%, MgO<0.5 wt%, Na_2O+K_2O=8.5–9.4 wt%, and Rb=70–90 ppm, Zr=830–960 ppm, Nb=110–130 ppm, Ba=630–710 ppm (Figs. 4 and 5).

Between the basaltic and rhyolitic end-members lie two compositional sub-groups. The first sub-group, with SiO_2=55.5–60.5 wt%, is represented by a scoria and a bomb embedded in a massive flood deposit at Holt (locality 2B; Fig. 2), an ignimbritic rock at Mosakambur (locality 4A; Fig. 2), and a mixed tephra exposed at Dyrhólaey (locality 2A; Fig. 2). These intermediate volcanic rocks of basaltic andesite to andesite composition are the result of magma mixing. They are characterised by
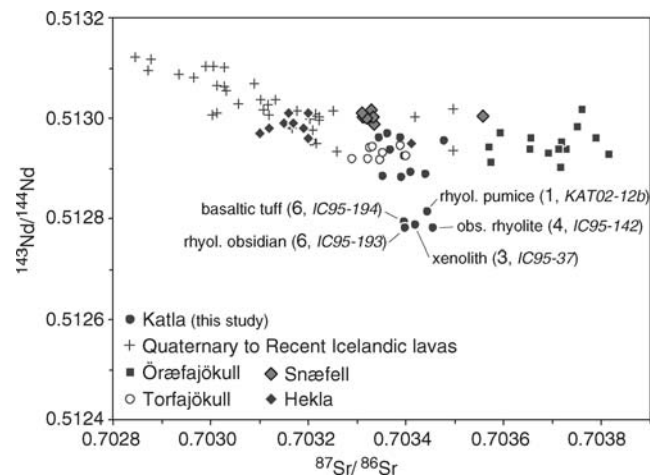
Fig. 8 Variation diagram of $^{87}Sr/^{86}Sr$ vs. $^{143}Nd/^{144}Nd$ ratios for Katla (TIMS whole-rock analyses, this study), Quaternary to Recent Icelandic lavas (Thirlwall et al. 2004), Öræfajökull (Prestvik et al. 2001), Snæfell (Hards et al. 2000), Torfajökull (Stecher et al. 1999), and Hekla (Sigmarsson et al. 1992). All data were normalised to the reference standards that were measured throughout the course of Katla sample analyses, averaging values of $^{87}Sr/^{86}Sr$=0.710235±9 for NBS 987 standard and $^{143}Nd/^{144}Nd$=0.5118220±8.5 for Johnson Matthey standard. In brackets, sampling area and identification of the Katla rock samples with low $^{143}Nd/^{144}Nd$ values (see Fig. 1 and Table 1)

TiO_2=2.0–2.9 wt%, Fe_2O_3=9.9–12.2 wt%, CaO=4.7–6.5 wt%, MgO=2.1–3.2 wt%, Na_2O+K_2O=5.6–6.8 wt%, and Rb=35–55 ppm, Y=60–75 ppm, Zr=510–630 ppm, Nb=65–85 ppm. A sub-group of dacitic composition with SiO_2=65.0–66.0 wt% is also attributed to magma mixing, and is represented by an obsidian clast at W. Húsargil (locality 1C; Fig. 2) and pumice and obsidian from a pyroclastic flow deposit at Vesturgil (locality 4C; Fig. 2). These samples are characterised by TiO_2=0.9±0.2 wt%, Fe_2O_3=7.4±0.4 wt%, CaO=3.0±0.1 wt%, MgO=0.9±0.2 wt%, Na_2O+K_2O=8.0±0.1 wt%, and Rb=65±1 ppm, Zr=802±3 ppm, Nb=102±1 ppm, Ba=585±15 ppm.

Concentrations of trace and rare earth (REE) elements measured by ICPMS on whole-rocks are listed in Table 1. Trace element concentrations were normalised against the C1 chondrite and N-MORB values from Sun and McDonough (1989). After normalisation to N-MORB values, mobile elements (Sr, K*, Rb, Ba) and immobile elements (Th, Ta, Nb, Ce, P*, Zr, Hf, Sm, Ti, Y, Yb) were arranged according to Pearce (1983). The analysed rocks are grouped as basaltic, intermediate (basaltic andesite, andesite, dacite) and rhyolitic rocks (Fig. 6), each of which is characterised by a restricted range of trace element contents. Basalts (SiO_2 ~45–52 wt%) show enrichment factors between 10 and 40 for mobile elements like Rb, and Ba, and less than 5 for immobile elements like Zr, Hf, Sm, Ti, Y, and Yb (N-MORB normalised). A negative P anomaly is apparent for all the basalts, suggesting apatite fractionation during crystallisation or apatite control during partial melting. The control of apatite in the differentiation becomes more pronounced for the rhyolites (SiO_2 ~68–72 wt%) and is shown by marked negative P anomalies (Fig. 6). Marked negative Ti anomalies also characterise the rhyolites and imply the involvement of Fe-Ti oxides

(titanomagnetite or ilmenite) in their differentiation, either during fractional crystallisation or partial melting. In contrast to the marked P and Ti negative anomalies, the N-MORB normalised trace element compositions of all rhyolites show very similar trace element patterns with enrichment factors of ~100–200 and less than 20, respectively, for mobile and immobile elements. The few rocks of intermediate composition (SiO_2 ~55–66 wt%) show concentrations intermediate between those for basalts and rhyolites. The narrow compositional range of normalised trace elements for basalts and rhyolites is also reflected by chondrite-normalised REE patterns (Fig. 6). Patterns for the basalts are roughly parallel and show similar shapes, with $(La/Sm)_n$=1.7–2.1 and $(Ce/Yb)_n$=5.8–6.7. This characteristic uniformity of REE patterns amongst Katla basalts was also observed by Meyer et al. (1985). The patterns of rhyolites show enrichment in LREE with $(La/Sm)_n$=2.7–3.2, without any significant change of the overall slope $(Ce/Yb)_n$=5.9–6.6. The few rocks of intermediate composition show parallel patterns including a slight LREE enrichment, with $(La/Sm)_n$=2.3–2.8. The role of plagioclase in the differentiation of intermediate rocks is illustrated by slight negative Eu anomalies characterised by Eu/Eu*=0.77–0.82. The negative Eu anomalies become more pronounced for rhyolites, with Eu/Eu*=0.60–0.71.

Binary diagrams of representative trace element concentrations (Ba vs. Sr and Rb vs. Sr) distinguish a basaltic and a rhyolitic end member (Fig. 7a, b). The rhyolites are characterised by narrow compositional fields whilst the basalts define a trend reflecting a probable combination of assimilation, melting or magma mixing, in addition to fractional crystallisation in their chemical differentiation. Sm/Nd vs. La/Yb and Dy/Yb vs. La/Yb trends extend this observation to the rhyolites (Fig. 7c, d).

Fig. 9 Variation diagrams of EMP glass compositions for **a** FeO_{tot}, Al_2O_3, CaO, **b** TiO_2, Na_2O and K_2O (wt%) vs. SiO_2 (wt%) on a water-free basis. **c**, **d** Expanded scale showing the different compositional groups of rhyolitic glass (**a**, **b**)
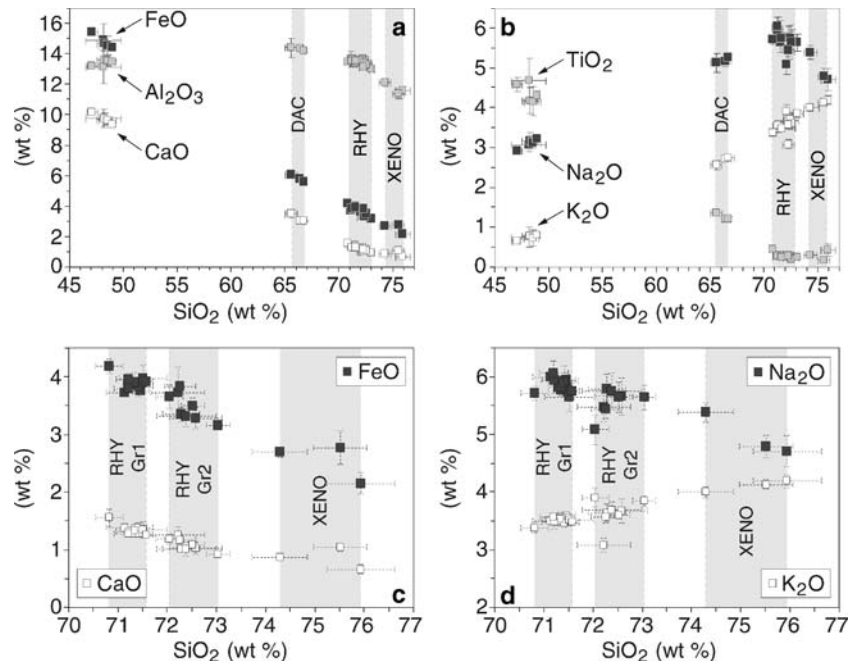
Sr/Nd isotopic ratios

The $^{87}Sr/^{86}Sr$ isotopes show a limited range from 0.703347 to 0.703479 within the overall variation for Iceland volcanic rocks and similar to the Torfajökull values, whilst the $^{143}Nd/^{144}Nd$ values range from 0.512780 to 0.512968 (Table 1; Fig. 8). The higher $^{143}Nd/^{144}Nd$ Katla values (0.512880–0.512968) compare with the Iceland trend, whilst the lowest values (0.512780–0.512813) are measured in a basaltic tuff (IC95-194), three rhyolitic extrusives (KAT02-12b, IC95-142, IC95-193) and a felsic xenolith (IC95-37). The Nd isotope value of the basaltic tuff may be suspect due to the possible remobilisation of the original deposit. However, Sr isotopes show a realistic ratio and therefore rule out alteration as a possible reason for the low Nd isotope value. The basaltic tuff deposit may have incorporated crustal material of low Nd values similar to that measured in the three rhyolitic extrusives and the xenolith. These low $^{143}Nd/^{144}Nd$ ratios measured in Katla rock specimens are among the lowest measured for Iceland,

and may be linked to assimilation and mixing of much older material from the wall rock of the magma reservoir.

Glass and mineral geochemistry

Major element composition of basaltic and silicic glasses

Table 2 lists the averaged major element compositions of glasses present in volcanic rocks (e.g. pumice, obsidian, fused xenolith, hyaloclastite, tephra) that were erupted from the Katla caldera. Each data point in Fig. 9a–d is the average of several (8–17) microprobe analyses (i.e. mean and standard deviation of the mean), and shows a fairly homogeneous and representative glass composition of the analysed sample. With the exception of the xenoliths, the variation in glass composition closely reproduces the whole-rock compositional trend (Fig. 9a, b), i.e. between a Fe-Ti transitional-alkali basalt end-member and a mildly alkali rhyolitic end-member. The compositional group of basaltic glasses (4.5<MgO<5.1 wt%) is characterised by mean concentrations of 4.1<TiO_2<4.7 wt%, 14.4< FeO_{tot}<15.4 wt%, and 9.3<CaO<10.2 wt% (Fig. 9a, b). However, major element concentrations derived from a single glass analysis can occasionally plot outside that compositional range, towards slightly more primitive or

Fig. 10 Compositional range of feldspars in rhyolitic rocks. *Number in brackets* refers to exposure (see Fig. 2). *In italic*, sample identification (see Table 1)
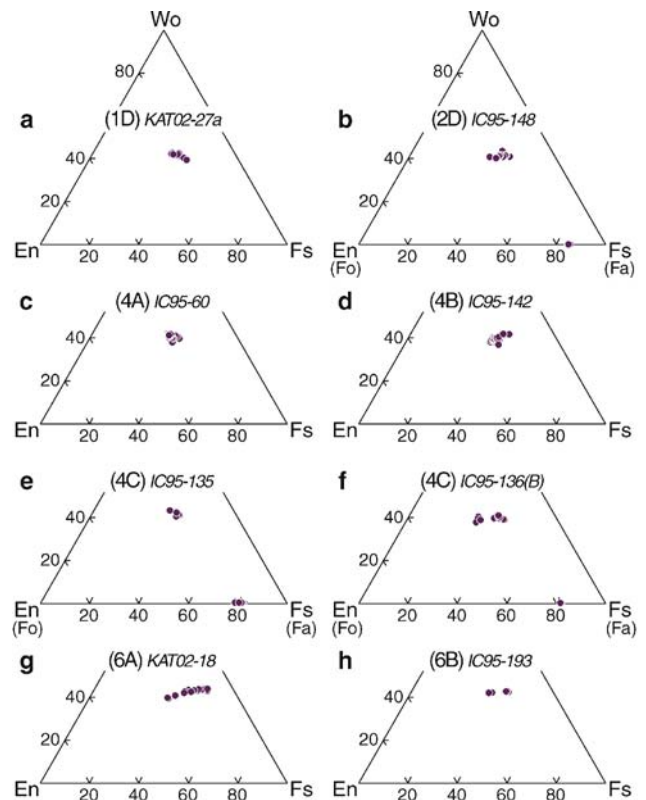
Fig. 11 Compositional range of clinopyroxene and co-existing olivine in rhyolitic rocks. *Number in brackets* refers to exposure (see Fig. 2). *In italic*, sample identification (see Table 1)

more evolved basaltic composition (see Fig. 5 in Lacasse et al. 1998).

Apart from interstitial glass in the fused xenoliths, the rhyolitic glasses can be divided into two groups that lie along the same compositional trend (Fig. 9c, d). Group 1 is characterised by mean concentrations of $70.8 < SiO_2 < 71.6$ wt%, $3.7 < FeO_{tot} < 4.2$ wt%, $1.2 < CaO < 1.6$ wt%, and $5.6 < Na_2O < 6.1$ wt%, whereas group 2 is characterised by mean concentrations of $72.0 < SiO_2 < 73.1$ wt%, $3.1 < FeO_{tot} < 3.9$ wt%, $0.9 < CaO < 1.3$ wt%, and $5.0 < Na_2O < 5.8$ wt% (Fig. 9c, d). The two compositional groups of rhyolitic glasses are also distinguished by the rock type and age. Group 1 mainly includes the rhyolitic products from the ~11.9 ka BP (Younger Dryas) major explosive eruption of Katla that are exposed as pyroclastic flow deposits up to ~10 m thick, e.g. at Dalárgil, Holsárgil, Húsárgil, Rjúpnagil (localities 1A-D; Fig. 2) and as a ~10–50 m thick deposit of coarse pyroclasts at Enta (locality 6C; Fig. 2). Group 2 mainly includes a ~30 cm thick interbedded tephra layer at Austurgil (locality 4A; Fig. 2) and a ~10 cm thick tephra layer exposed in a gully near Oddnýjartjörn lake (locality 2C; Fig. 2). These two tephra layers were correlated on geochemical grounds. The proximal tephra at Austurgil, by the southern Mýrdalsjökull ice margin, is overlain by hyaloclastite, indicating a probable older age than that of the ~11.9 ka BP major eruption.

Glasses of dacitic composition lie along the trend defined between the basaltic and rhyolitic groups, with $65.5 < SiO_2 < 66.8$ wt%, $5.5 < FeO_{tot} < 6.1$ wt%, $3.0 < CaO < 3.5$ wt%, and $5.1 < Na_2O < 5.3$ wt% (Fig. 9a, b). This narrow compositional range characterises three silicic tephras recovered in a soil section in the northern half of sampling area 3 (Fig. 1) that were previously ^{14}C dated at 3139±40 years BP (tephra SILK-LN), 2975±12 years BP (tephra SILK-MN), and 2660±50 years BP (tephra SILK-UN; Larsen et al. 2001). The same compositional range also closely reflects the glass composition of 12 silicic tephras in total that were erupted between ~6,600 and 1675 years ^{14}C BP (Larsen et al. 2001).

The interstitial glass of three partly fused felsic xenoliths was also analysed. The xenoliths represent incompletely crystallised (or partially fused) relics of a magma chamber rind or solidification front, and that were entrained by the ascending magma during eruption. Such relics can be found quite commonly in arc magmas (Brown et al. 1998; Burt et al. 1998). Compositions of the analysed interstitial glasses plot at the silica-rich end of the rhyolitic glass trend, with $74.0 < SiO_2 < 75.5$ wt%, $2.1 < FeO_{tot} < 2.8$ wt%, $0.6 < CaO < 1.1$ wt%, and $4.6 < Na_2O < 5.4$ wt% (Fig. 9c, d), exceeding by up to 5 wt% the whole-rock silica content in the same felsic xenoliths.

Chemical variation of feldspars and pyroxenes in rhyolitic rocks

The composition of feldspar phenocrysts was studied in rhyolitic rocks that are exposed either as lavas or pyroclasts around the rim of the Katla caldera. The youngest (~11.9 ka BP) of these rhyolitic rock formations are represented by exposures of pyroclastic flow deposits on either side of the Sólheimajökull glacier (localities 1A-D; Fig. 2). Phenocryst contents in pumices and obsidian clasts are less than 5%. Feldspars from a pyroclastic flow deposit in Dalárgil (locality 1A; Fig. 2) show a dominant composition of oligoclase (An_{20-24}; Fig. 10a). A broader composition variation (An_{19-42}) from oligoclase to andesine was measured in feldspars from a pumice derived from another flow deposit in Rjúpnagil (locality 1D; Figs. 2 and 10b). Feldspars from an interbedded pumice layer in Steigarhals (locality 2D; Fig. 2) show a homogeneous oligoclase composition of An_{13-21} slightly higher in sodium (Fig. 10c). Oligoclase composition of three out of four rhyolitic rock samples, collected between Austurgil and Vesturgil (localities 4A-C; Fig. 2), vary from An_{17-22} to An_{21-24} (Fig. 10d–f). A pillow-shaped obsidian from Vesturgil (locality 4C; Fig. 2) contains enclaves of mafic (basaltic?) composition, up to ~1 cm size, and phenocrysts of oligoclase (An_{16-22}) and andesine (An_{32-34}) composition (Fig. 10f). The predominant oligoclase composition of the rhyolitic series is also found in crystal-poor (<5%) pumices and obsidians from above Huldufjöll (locality 5A; Fig. 2) and from Enta (locality 6C; Fig. 2), and in a rhyolitic obsidian from Bláfell (locality 6B; Fig. 2), with feldspar composition of An_{20-24}, An_{19-22}, and An_{19-24}, respectively (Fig. 10h, j, k). A crystal-rich rhyolite (~20–30%) from Austmannsbunga (locality 6A; Fig. 2) differs from the entire series by containing large phenocrysts of up to 3 mm in size that are partially resorbed, with a broad compositional range from oligoclase (An_{24}) to sodic anorthoclase ($Ab_{79}Or_{14}An_7$; Fig. 10i).

Clinopyroxene phenocrysts were found co-existing with feldspars in eight of the eleven rhyolitic samples that were studied. The clinopyroxenes are represented by greenish ferroaugite (Fs >30 mol%) mainly characterised by a narrow compositional range, e.g. $Wo_{39-43}En_{21-26}Fs_{32-40}$ for a pumice from a pyroclastic flow deposit at Rjúpnagil (locality 1D; Figs. 2 and 11a). Pyroxenes in four rhyolitic rocks from the Gvendarfell area (localities 4A-C; Fig. 2) also show an overall narrow composition range of $Wo_{37-43}En_{18-34}Fs_{28-41}$ (Fig. 11c–f), similar to that of an obsidian from Bláfell (locality 6B; Fig. 2) with $Wo_{42-43}En_{18-26}Fs_{32-40}$ (Fig. 11h). The crystal-rich rhyolite from Austmannsbunga (locality 6A; Fig. 2) can be considered apart, as previously observed on the basis of its feldspar composition, with a relatively broad compositional range of clinopyroxene with $Wo_{39-44}En_{11-29}Fs_{32-46}$ (Fig. 11g). These clinopyroxenes show the largest compositional Fs variation (14 mol%) of the whole rhyolitic series. Fe-rich olivine phenocrysts were found co-existing with clinopyroxenes and feldspars in three of the studied rhyolitic rock samples (Fig. 11b, e, f), with Fo_{14}-Fo_{15}, Fo_{17}-Fo_{21}, Fo_{18}, in a pumice from an interbedded layer in Steigarháls (locality 2D; Fig. 2), in a pillow-shaped obsidian, and in a pumice from a pyroclastic flow unit from the Vesturgil area (locality 4C; Fig. 2), respectively.

Discussion

Magma bimodality and mixing

The Katla volcanic complex is characterised by a strongly bimodal magma suite consisting of high-Ti transitional basalts and rhyolites. For consistency we use the same terminology as Sparks and Marshall (1986) to describe and interpret the different processes related to magma mixing. Magma mingling occurs when magmas are mixed together physically but compositional heterogeneities (i.e. enclaves) are preserved in the rock product. Magma hybridisation occurs when magmas are mixed together to form a completely blended homogeneous mixed magma.

Based on whole-rock and glass chemistry, the Katla volcanic rock series shows a uniform chemical trend from Fe-Ti transitional basalts to mildly alkalic rhyolites (Figs. 4, 5 and 9). Narrow compositional ranges for major and trace elements characterise the two basaltic and rhyolitic end-members (Table 1; Figs. 4 and 5). As illustrated by the spider diagrams of Fig. 6, each end-member shows a great uniformity in their normalised trace and rare earth element concentrations that indicates a common petrogenetic link amongst the basalts and the rhyolites. The few examples of intermediate bulk composition in the Katla rock series are mainly derived from magma mingling. There are, however, a few examples of hybridisation as shown by the compositions of dacitic glass (SILK tephras, ~2–7 ka BP) and possibly of rhyolitic glass group 1 (~11.9 ka BP). These two distinct compositional groups plot on the general Katla chemical trend linking the basaltic and the most evolved rhyolitic glass compositions. There is a large compositional gap between each group which is difficult to explain by fractional crystallisation (Fig. 9).

Petrogenesis of felsic xenoliths and rhyolitic extrusives

Felsic xenoliths of rhyolitic bulk composition were found at the Katla caldera, often associated with rhyolitic extrusives (e.g. pyroclastic flows; Table 1). They represent fragments of crustal rocks that have experienced various stages of crystallisation or partial melting prior to quenching. They were probably removed from a magma reservoir rind or solidification front and entrained by the ascending magma during eruption. Felsic xenoliths are relatively common in Icelandic volcanics (e.g. Sigurdsson 1968) and their origin has been debated for some time. Based on theoretical and experimental studies, rhyolites can be formed in the Icelandic crust either by single-stage >90% fractional crystallisation of transitional basaltic magmas (e.g. MacDonald et al. 1990) or by partial melting of hydrated basaltic rocks (e.g. Thy et al. 1990). Considering that a massive gabbroic intrusive complex (~1,000 km^3) exists in the upper crust underneath the Katla caldera

(Gudmundsson 1994), a volume of rhyolitic melt in excess of several km^3 could have easily been produced by single-stage fractional crystallisation (e.g. by simple crystal settling), but not without also generating a significant proportion of melts and extrusive rocks of intermediate composition. In the case of Katla, there is no support for the fractional crystallisation hypothesis as reflected by the large compositional gap between the erupted basalt and rhyolitic melts (Fig. 9), with the rare extrusives of intermediate bulk composition (Figs. 4 and 5) found to result from magma mingling (Fig. 3a–c). The occurrence of hydrous minerals (amphiboles, see Fig. 3e) in some of the crustal felsic xenoliths from Katla favours the second hypothesis involving partial melting of metamorphosed or hydrated parts of the Icelandic basalt crust (amphibolite) for the generation of rhyolitic melt. The generation of melts of intermediate (andesitic, dacitic) composition by the same process (see Figs. 1, 2 and 3 in Thy et al. 1990) remains nevertheless questionable until hydrated crustal xenoliths of intermediate composition, as at Torfajökull (e.g. sample T-33X in Gunnarsson et al. 1998), are found at Katla. The absence of amphibole crystals in rhyolitic extrusives could be due to their breakdown and the release of volatiles (H_2O) during the late crystallisation phase and prior to eruption.

Electron microprobe analyses of rhyolitic glass from fused xenoliths and glassy extrusives (pumice, obsidian, tephra) clearly show that they are probably genetically linked (Fig. 9). Extrusives with the less evolved rhyolitic composition (group 1) can be derived from the hybridisation of melts of rhyolitic group 2 and basaltic (or dacitic) compositions. Intruding basaltic magma is the most plausible heat source for melting the hydrated basaltic crust. Incipiently welded pyroclastic flows (Sólheimar ignimbrite), agglutinate obsidian textures and crystal-poor pumice contents are indicative of the low viscosity of the rhyolitic magma extruded for example during the large explosive eruption, ~11.9 ka BP, and suggest that it may have been superheated by the same mechanism.

Conclusions

Our study, based on the petrographic and geochemical analyses of lavas and pyroclastic rocks, brings new information on the melt genesis of past major Katla rhyolitic eruptions and into other magmatic processes occurring beneath the subglacial caldera. The Katla volcanic rock series is characterised by a well-defined bimodal composition that includes Fe-Ti transitional-alkali basalts and mildly alkalic rhyolites. It is, together with the Askja and Öræfajökull rock-series (Prestvik 1980; Sigurdsson and Sparks 1981), one of the clearest examples of mixed magma series in Iceland.

Each of the two Katla end-members shows a narrow compositional range in major elements and uniform

normalised patterns (spider diagrams) of mobile and immobile trace elements (including REE). Linear trends for specific trace element ratios are observed amongst the basalts and rhyolites, and suggest that fractional crystallisation was the main process leading to the chemical differentiation within the end-member magmas. Apatite is among the early crystallising phases controlling the chemical differentiation of basalts as shown by negative P anomalies, becoming more pronounced for rhyolites. Negative Ti and Eu anomalies observed for rhyolites imply the additional control of Fe-Ti oxides and plagioclase feldspar in their differentiation by fractional crystallisation.

Between the basaltic and rhyolitic end-members lie a few rock specimens of intermediate whole-rock composition separated by compositional gaps. Their petrography shows evidence of mingling of distinct mafic and silicic magma components. Textural heterogeneity of the intermediate rock products is preserved as indicated by the occurrence of dark (mafic) microcrystalline enclaves. Similar enclaves of mafic texture are occasionally found in smaller amount in rhyolitic rocks.

The same compositional bimodality is recorded in the glass analyses of pyroclastic rocks, with large gaps between basaltic, dacitic, and rhyolitic glasses. Rhyolitic glasses from pyroclasts and tephras fall into two distinct compositional groups which are mainly derived from two explosive silicic eruptions that occurred after the Last Glacial Maximum (~20 ka BP), including the main source of the rhyolitic components of Ash Zone 1 and the Vedde Ash (Younger Dryas, ~11.9 ka BP) in the North Atlantic. The two pyroclastic glass populations lie in continuity with the compositional trend of rhyolitic glass from fused xenoliths, suggesting that they are linked by partial melting and possible magma hybridisation later on. Only intermediate glasses of homogeneous dacitic composition were found lying along the same trend, with large compositional gaps separating them from the basaltic and rhyolitic glass end-members. The dacitic glasses were probably derived from complete magma mixing and chemical homogenisation (hybridisation) and were associated with an episode of silicic explosive volcanism that occurred between 2 and 7 ka BP.

The absence of xenoliths of intermediate magmatic composition and the occurrence of hydrous minerals (amphibole) in felsic xenoliths favour the hypothesis of partial melting of hydrated parts of the Icelandic basalt crust (amphibolite) rather than the hypothesis of fractional crystallisation of basalts. The absence of hydrous minerals (amphibole) in rhyolitic extrusives indicates that amphibole breakdown and possible release of volatiles (H_2O) may have occurred during the late crystallisation phase and prior to eruption. Low Nd isotope ratios of a few rhyolitic rock specimens (extrusives and xenoliths) suggest the possible assimilation and mixing of much older crustal material during the overall petrogenetic process.

References

Björnsson H, Pálsson F, Gudmundsson MT (2000) Surface and bedrock topography of the Mýrdalsjökull ice cap, Iceland. Jökull 49:29–46

Blake S (1984) Magma mixing and hybridisation processes at the alkalic, silicic, Torfajökull central volcano triggered by tholeiitic Veidivötn fissuring, south Iceland. J Volcanol Geotherm Res 22:1–31

Brown SJA, Burt RM, Cole JW, Krippner SJP, Price RC, Cartwright I (1998) Plutonic lithics in ignimbrites of Taupo Volcanic Zone, New Zealand: sources and conditions of crystallisation. Chem Geol 148:21–41

Burt RM, Brown SJA, Cole JW, Shelley D, Waight TE (1998) Glass-bearing plutonic fragments from ignimbrites of the Okataina caldera complex, Taupo Volcanic Zone, New Zealand: remnants of a partially molten intrusion associated with preceding eruptions. J Volcanol Geotherm Res 84:209–237

Carmichael ISE (1964) The petrology of Thingmuli, a Tertiary volcano in eastern Iceland. J Petrol 5:435–460

Eggins SM, Woodhead JD, Kinsley LPJ, Sylvester P, McCulloch MT, Hergt JM, Handler MR (1997) A simple method for the precise determination of 40 or more trace elements in geological samples by ICP-MS using enriched isotope internal standardisation. Chem Geol 132:311–326

Einarsson P, Brandsdóttir B (2000) Earthquakes in the Mýrdalsjökull area, Iceland, 1978–1985: seasonal correlation and connection with volcanoes. Jökull 49:59–73

Furman T, Frey FA, Meyer PS (1992) Petrogenesis of evolved basalts and rhyolites at Austurhorn, southeastern Iceland: the role of fractional crystallisation. J Petrol 33:1405–1445

Govindaraju K, Potts PJ, Webb PC, Watson JS (1994) 1994 report on Whin Sill dolerite WS-E from England and Pitscurrie microgabbro PM-S from Scotland: assessment by one hundred and four international laboratories. Geost Newsl 18:211–300

Grönvold K, Oskarsson N, Johnsen SJ, Clausen HB, Hammer CU, Bond G, Bard E (1995) Ash layers from Iceland in the Greenland GRIP ice core correlated with oceanic and land sediments. Earth Planet Sci Lett 135:149–155

Gudmundsson MT (1994) The structure of Katla, a central volcano in a propagating rift zone, South Iceland, from gravity data. EOS Trans AGU 75, Spring Meet Suppl, T22C-4

Gunnarsson B, Marsh BD, Taylor Jr HP (1998) Generation of Icelandic rhyolites: silicic lavas from the Torfajökull central volcano. J Volcanol Geotherm Res 83:1–45

Hards VL, Kempton PD, Thompson RN, Greenwood PB (2000) The magmatic evolution of the Snæfell volcanic centre: an example of volcanism during incipient rifting in Iceland. J Volcanol Geotherm Res 99:97–121

Hildebrand L, Grönvold K, Oskarsson N (1998) Geochemistry and evolution of the Katla volcanic centre, south Iceland. Nordic Volcanological Institute, Reykjavik, Abstract

Jakobsson SP (1979) Petrology of recent basalts of the Eastern Volcanic Zone, Iceland. Acta Nat Isl 26

Jónsson J (1982) Notes on Katla volcanoglacial debris flows. Jökull 32:61–68

Lacasse C, Garbe-Schönberg C-D (2001) Explosive silicic volcanism in Iceland and the Jan Mayen area during the last 6 Ma: source and timing of major eruptions. J Volcanol Geotherm Res 107:113–147

Lacasse C, Sigurdsson H, Jóhannesson H, Paterne M, Carey SN (1995) Source of Ash Zone 1 in the North Atlantic. Bull Volcanol 57:18–32

Lacasse C, Carey SN, Sigurdsson H (1998) Volcanogenic sedimentation in the Iceland Basin: influence of subaerial and subglacial eruptions. J Volcanol Geotherm Res 83:47–73

Lacasse C, Thomas LE, Björnsson H, Gudmundsson MT, Gudmundsson H (2002) Potential hazards to Great Britain from major explosive eruptions: a cross-disciplinary study of the subglacial Katla volcano (S. Iceland). In: Proc Chapman Conf on Volcanism and the Earth's Atmosphere, June 2002, Thera, Greece, Abstract, p 41

Larsen G (2000) Holocene eruptions within the Katla volcanic system, south Iceland: characteristics and environmental impact. Jökull 49:1–28

Larsen G, Newton AJ, Dugmore AJ, Vilmundardóttir EG (2001) Geochemistry, dispersal, volumes and chronology of Holocene silicic tephra layers from the Katla volcano system, Iceland. J Quat Sci 16:119–132

Le Bas MJ, Le Maitre RW, Streckeisen A, Zanettin B (1986) A chemical classification of volcanic rocks based on the total alkali-silica diagram. J Petrol 27:745–750

MacDonald R, McGarvie DW, Pinkerton H, Smith RL, Palacz ZA (1990) Petrogenetic evolution of the Torfajökull volcanic complex, Iceland: I. Relationships between the magma types. J Petrol 31:429–459

Maizels J (1991) The origin and evolution of Holocene sandur deposits in areas of jökulhlaup drainage, Iceland. In: Maizels JK, Caseldine C (eds) Environmental change in Iceland: past and present. Kluwer, Dordrecht, pp 267–302

McGarvie DW (1984) Torfajökull: a volcano dominated by magma mixing. Geology 12:685–688

McGarvie DW, MacDonald R, Pinkerton H, Smith RL (1990) Petrogenetic evolution of the Torfajökull volcanic complex, Iceland: II. The role of magma mixing. J Petrol 31:461–481

Meyer PS, Sigurdsson H, Schilling J-G (1985) Petrological and geochemical variations along Iceland's neovolcanic zones. J Geophys Res 90:10043–10072

Nielsen CH, Sigurdsson H (1981) Quantitative methods for electron microprobe analysis of sodium in natural and synthetic glasses. Am Mineral 66:547–552

Oladóttir B, Larsen G, Thordarson Th, Sigmarsson O (2005) The Holocene eruption history and magmatic evolution at the Katla volcanic system, Iceland. EGU Geophys Res Abstracts 7, EGU, Vienna, p 816

Oskarsson N, Sigvaldason GE, Steinthórsson S (1982) A dynamic model of rift zone petrogenesis and the regional petrology of Iceland. J Petrol 23:28–74

Oskarsson N, Steinthórsson S, Sigvaldason GE (1985) Iceland geochemical anomaly: origin, volcanotectonics, chemical fractionation and isotope evolution of the crust. J Geophys Res 90:10011–10025

Pearce JA (1983) The role of sub-continental lithosphere in magma genesis at destructive plate margins. In: Hawkesworth CJ, Norry MJ (eds) Continental basalts and mantle xenoliths. Nantwich, Cheshire, UK, pp 230–249

Potts PJ, Tindle AG, Webb PC (1992) Geochemical reference material compositions. CRC Press, Boca Raton, FL

Prestvik T (1980) Petrology of hybrid intermediate and silicic rocks from Öræfajökull, southeast Iceland. Geol Fören Stockholm Förh 101:299–307

Prestvik T, Goldberg S, Karlsson H, Grönvold K (2001) Anomalous strontium and lead isotope signatures in the off-rift Öræfajökull central volcano in south-east Iceland-Evidence for enriched endmember(s) of the Iceland mantle plume? Earth Planet Sci Lett 190:211–220

Robson GR (1957) The volcanic geology of Vestur-Skaftafellssýsla, Iceland. PhD Thesis, University of Durham

Sigmarsson O, Hémond C, Condomines M, Fourcade S, Oskarsson N (1991) Origin of silicic magma in Iceland revealed by Th isotopes. Geology 19:621–624

Sigmarsson O, Condomines M, Fourcade S (1992) A detailed Th, Sr and O isotope study of Hekla: differentiation processes in a Icelandic volcano. Contrib Mineral Petrol 112:20–34

Sigmarsson O, Oladóttir B, Larsen G, Thordarson Th (2005) Temporal variations of trace element ratios in basaltic tephra from Katla volcano, Iceland: a reconnaissance study. EGU Geophys Res Abstracts 7, EGU, Vienna, p 10182

Sigurdsson H (1968) Petrology of acid xenoliths from Surtsey. Geol Mag 105:440–453

Sigurdsson H (1970) The petrology and chemistry of the Setberg volcanic region and of the intermediate and acid rocks of Iceland. PhD Thesis, University of Durham

Sigurdsson H (1977) Generation of Icelandic rhyolites by melting of plagiogranites in the oceanic layer. Nature 269:25–28

Sigurdsson H, Sparks RSJ (1981) Petrology of rhyolitic and mixed magma ejecta from the 1875 eruption of Askja, Iceland. J Petrol 22:41–84

Sparks RSJ, Marshall LA (1986) Thermal and mechanical constraints on mixing between mafic and silicic magmas. J Volcanol Geotherm Res 29:99–124

Stecher O, Carlson RW, Gunnarsson B (1999) Torfajökull: a radiogenic end-member of the Iceland Pb-isotopic array. Earth Planet Sci Lett 165:117–127

Sturkell E, Sigmundsson F, Einarsson P (2003a) Recent unrest and magma movements at Eyjafjallajökull and Katla volcanoes, Iceland. J Geophys Res 108(B8):2369. DOI 10.1029/2001JB000917

Sturkell E, Sigmundsson F, Einarsson P, Geirsson H, Roberts MJ (2003b) Magma inflow into Katla, one of Iceland's most hazardous volcanoes. EOS Trans AGU 84(46), Fall Meet Suppl, F1503

Sun S-S, McDonough WF (1989) Chemical and isotopic systematics of oceanic basalts: implications for mantle composition and processes. In: Saunders AD, Norry MJ (eds) Magmatism in the ocean basins. Geol Soc London Spec Publ 42:313–346

Sæmundsson K (1979) Outline of the geology of Iceland. Jökull 29:7–28

Thirlwall MF, Gee MAM, Taylor RN, Murton BJ (2004) Mantle components in Iceland and adjacent ridges investigated using double-spike Pb isotope ratios. Geochim Cosmochim Acta 68:361–386

Thompson M, Potts PJ, Webb PC (1996) GeoPT1. International proficiency test for analytical geochemistry laboratories-report on round 1 (July 1996). Geost Newsl 20:295–325

Thordarson Th, Miller DJ, Larsen G, Self S, Sigurdsson H (2001) New estimate of sulphur degassing and atmospheric mass-loading by the 934 AD Eldgjá eruption, Iceland. J Volcanol Geotherm Res 108:33–54

Thy P, Beard JS, Lofgren GE (1990) Experimental constraints on the origin of Icelandic rhyolites. J Geol 98:417–421

Wastergard S, Turney CSM, Lowe JJ, Roberts SJ (2000) New discoveries of the Vedde Ash in southern Sweden and Scotland. Boreas 29:72–78

Watson JS (1996) Fast, simple method of powder pellet preparation for X-ray fluorescence analysis. X-Ray Spectr 25:173–174

Wood DA (1978) Major and trace element variations in the Tertiary lavas of eastern Iceland and their significance with respect to the geochemical anomaly. J Petrol 19:393–436